AD-A175 026 FLOW THROUGH A COMPRESSOR STAGE(U) SCIENTIFIC RESEARCH 1/1
ASSOCIATES INC GLASTONBURY CT H J GIBELING ET AL
MAY 86 R86-910004-F AFOSR-TR-86-2181 F49620-83-C-0119
UNCLASSIFIED F/G 20/4 NL

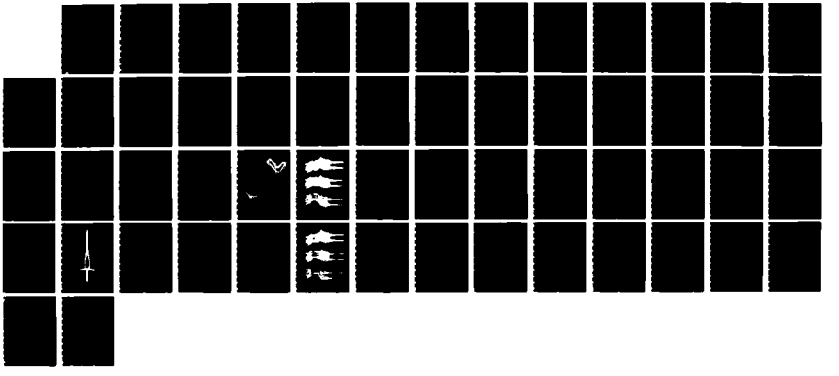

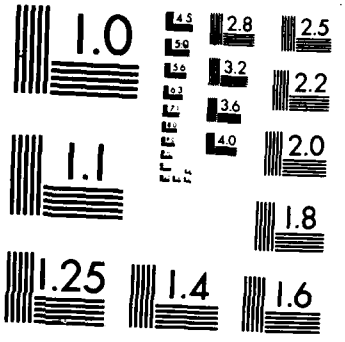

SECURITY CLASSIFICATION OF THIS PAGE *(When Data Entered)*

REPORT DOCUMENTATION PAGE		READ INSTRUCTIONS BEFORE COMPLETING FORM
1. REPORT NUMBER AFOSR-TR- 86-2181	2. GOVT ACCESSION NO.	3. RECIPIENT'S CATALOG NUMBER
4. TITLE *(and Subtitle)* FLOW THROUGH A COMPRESSOR STAGE		5. TYPE OF REPORT & PERIOD COVERED Final Report 6/21/83 - 5/31/86
		6. PERFORMING ORG. REPORT NUMBER R86-910004-F
AUTHOR(s) H.J. Gibeling, B.C. Weinberg S.J. Shamroth and H. McDonald		8. CONTRACT OR GRANT NUMBER(s) F49620-83-C-0119
PERFORMING ORGANIZATION NAME AND ADDRESS Scientific Research Associates, Inc. P.O. Box 498 Glastonbury, CT 06033		10. PROGRAM ELEMENT, PROJECT, TASK AREA & WORK UNIT NUMBERS 61102F 2307 A4
CONTROLLING OFFICE NAME AND ADDRESS Air Force Office of Scientific Research Bolling Air Force Base, DC 20332 NA		12. REPORT DATE May 1986 13. NUMBER OF PAGES
MONITORING AGENCY NAME & ADDRESS *(if different from Controlling Office)* Same as 11		15. SECURITY CLASS. *(of this report)* Unclassified 15a. DECLASSIFICATION/DOWNGRADING SCHEDULE

16. DISTRIBUTION STATEMENT *(of this Report)*

Approved for public release;
distribution unlimited.

17. DISTRIBUTION STATEMENT *(of the abstract entered in Block 20, if different from Report)*

Approved for public release;
distribution unlimited.

DTIC ELECTE DEC 1 2 1986

18. SUPPLEMENTARY NOTES

19. KEY WORDS *(Continue on reverse side if necessary and identify by block number)*

Stage Analysis, Cascade, Time-Dependent Navier-Stokes, Compressor

20. ABSTRACT *(Continue on reverse side if necessary and identify by block number)*

A two-dimensional, time-dependent Navier-Stoke calculation procedure is applied to the problem of flow through a stator-rotor stage. The case considered is a stage formed by two supercritical type compressor blades. The grid is a single grid about the stage consisting of a 'C' grid about the leading stator blade, an 'H' grid about the trailing rotor blade and a

DD FORM 1 JAN 73 1473 EDITION OF 1 NOV 65 IS OBSOLETE

Scientific Research Associates, inc.

P. O. Box 498
Glastonbury, Connecticut 06033

FLOW THROUGH A COMPRESSOR STAGE

H.J. Gibeling
B.C. Weinberg
S.J. Shamroth
H. McDonald

Scientific Research Associates, Inc.
Final Report Prepared for Air Force Office of Scientific Research
Under Contract F49620-83-C-0019

May 1986

TABLE OF CONTENTS

A-1

INTRODUCTION

One major consideration driving modern aircraft gas turbine engine designs is the desire to increase the thrust-to-weight ratio. This, in turn, requires more highly loaded compressor and turbine stages with concern for optimum spacing between adjacent blade passages. With this motivation, the fluid dynamic processes in typical turbine and compressor blade passages and stages have become an item of considerable importance. The aerodynamic behavior of these components can have a major effect upon the overall engine efficiency. In addition, details of the flow pattern can significantly influence structural integrity via unsteady forces produced by the relative blade motion and, in the case of the turbine, by influencing the leading edge heat transfer rates.

To date, considerable attention has been focused upon single blade passage flows. For example, Dring, Joslyn and Hardin (Ref. 1); Wagner, Dring and Joslyn (Ref. 2); Joslyn and Dring (Ref. 3); and Shreeve and Neuhoff (Ref. 4) have performed detailed investigations in compressor rotors and stators. Linear cascades have been considered by Hobbs, Wagner, Dannenhoffer and Dring (Ref. 5), among others. In regard to the single passage flow field, Navier-Stokes procedures have been applied to this problem by several investigators including Shamroth, McDonald and Briley (Ref. 6); Hah (Ref. 7); Weinberg, Yang, McDonald and Shamroth (Ref. 8); Schafer, Fruhaufer, Bauer and Guggolz (Ref. 9); and Dawes (Ref. 10). These efforts include both two-dimensional and three-dimensional analyses (Refs. 7 and 8). The two-dimensional analyses of Refs. 6, and 8 through 10 are based upon ADI solutions of the Navier-Stokes equations. Schafer, et al., (Ref. 9) considered Euler solutions for flow through a cascade of NACA-0012 airfoils, as well as both Navier-Stokes and "thin shear layer" solution for flow through a cascade of NACA-8410 airfoils. Although convergence comments were made in regard to Euler cascade solutions presented in this paper; for example, a cascade of 0012 airfoils at zero degree stagger appeared to require approximately 400 to 600 time steps to converge, the number of time-steps to converge their "thin shear layer" or Navier-Stokes calculation was not clear. Dawes (Ref. 10) also used an ADI approach to solve the Navier-Stokes equations for flow in transonic compressor cascades; in this case 400-600 time steps are required to converge. Both Refs. 9 and 10 considered compressor type cascades with

thin blades and relatively little turning. In contrast, Refs. 6 and 8, which were performed with earlier versions of the code used here, considered both compressor cascades and turbine cascades. The latter, having blunter leading edges, higher stagger angles and more turning, become a more difficult and challenging simulation problem. Calculations performed recently with this code required 80-120 time steps to convergence, with run time per time step for the grids used being approximately 0.4 CPU seconds. Solutions were obtained in 30 to 70 CPU seconds of Cray-I time using grids containing 3500 points. In Ref. 7, Hah took a different approach, using a control volume relaxation approach to solving the Navier-Stokes equations. However, the equations being solved by a relaxation procedure are limited to a steady mean flow. It may be possible to extend such a procedure to unsteady flow, however, such an extension would require iteration at each time step, which would increase run time significantly.

Although considerable information can be gained by considering the flow through a single row of blades, a more complex and potentially more important problem is that of the flow through a stator-rotor stage. Such an investigation would include the potentially important interaction between adjacent blade passages. Information obtained from a stage investigation could contain important flow physics not addressed in a single blade row investigation. To date, considerably less effort has focused upon the stage problem. In regard to experimental efforts, Detroit Diesel Allison has studied various aspects of unsteady flow in a compressor stage with the primary emphasis being the time-variant aerodynamics of the stator as a function of rotor-stator spacing, solidity, etc. (Refs. 11-14). Dring, Joslyn, Hardin and Wagner (Ref. 15) have considered the effect of axial spacing upon the turbine stage flow field.

In regard to analysis, the rotor-stator stage calculation is considerably more demanding than a single blade row passage calculation. In the stage, the flow is intrinsically unsteady and, therefore, transient accuracy is required. Furthermore, the computational grid required for a stage is considerably more complex than that for a single passage analysis. To date, two stage calculation procedures which are based upon solution of the Navier-Stokes equations have been developed. They are the procedure of Rai (Ref. 16) and the procedure reported herein. Both efforts considered the same basic problem, that of a time dependent, two-dimensional Navier-Stokes

simulation of flow through a stage. The major differences between the two were the computational coordinate systems and the numerical techniques used. Prior to considering the details of the present analysis, it is useful to compare the similarities and differences of the present approach with that of Ref. 16 in a general manner.

In regard to the computational grids used, Rai used a combination of patched and overlaid grids, as shown in Fig. 1, which is taken from Ref. 16. The blade geometries are shown in Fig. 1a. Figure 1b shows 'O' grids in the immediate vicinity of each blade. Each 'O' grid is embedded within an 'H' grid where the 'H' grids are shown in Fig. 1c. The general patching and overlay is shown in Fig. 1d. Although this approach can give a highly resolved grid through the flow field, the overlay between regions 1 and 2, and regions 3 and 4, requires a technique to specify boundary conditions on the inner boundaries of zones 3 and 4, and the outer boundaries of zones 1 and 2. This basically requires some method of applying "boundary conditions" on a computational line internal to the flow field. Rai has successfully approached this problem by an iterative procedure in which outer zone 1 and and 2 boundary points are interpolated from zone 3 and 4 results, and inner zone 3 and 4 boundary points are interpolated from zone 1 and 2 results. Although this approach has been successful, it does require additional iteration within the calculation which, in turn, increases computer run time. In addition, the overlapped multiple patched grids may require more grid points than a single non-overlaid grid for each blade. Finally, the use of these internal line boundary conditions may introduce a stability limit on the allowable time step which can be taken. Along the patched boundaries a somewhat similar approach is used in which an iterative solution between zones is combined with conservation of fluxes across a patch line. A major advantage of this approach is that it allows a relatively small gap between rotor and stator to be considered.

In the approach detailed in the present report, a key priority was development of an efficient stator-rotor stage calculation procedure which would require a minimum run time. Minimization of run time was considered critical for several reasons. First, even for the simplest stage calculation, which is two-dimensional and assumes equal pitch in rotor and stator, four to eight cycles are expected to be required to obtain a periodic solution. A cycle is defined as the time required for the rotor to move a

distance equal to one pitch. The goal of the present effort was to develop a stage Navier-Stokes simulation technique which would lead to periodic solutions for the two-dimensional, equal pitch configurations in a modest amount of computer run time to allow stage calculations to be made on a regular basis. Secondly, the eventual interest is in either three-dimensional stage simulations or simulations in which rotor and stator have unequal number of blades, i.e., unequal pitch. The three-dimensional simulation is expected to require sixty times the computer time of the simple two-dimensional calculation and the two-dimensional unequal blade calculation is expected to require twenty to forty times the computer run time of the simple two-dimensional calculation. If these are to be approached on anything but a research demonstration-type basis, the basic two-dimensional equal pitch case must be very efficient in use of computer resources.

Both a single grid approach and a patched grid approach were considered. The trade-off appeared to be the single grid advantage of rapid run time versus the small gap spacing ability of the patched grid approach. Since one important application of the procedure would be compressor technology, and since a compressor stage gap of approximately 25% axial chord appears to be viable with the single grid approach, the single grid approach was chosen. As will be discussed, this has led to a very efficient procedure which would require only 2 CPU minutes of CRAY time per cycle and 10 minutes to obtain a periodic solution. This appears, at the present time, to be significantly faster than the run times achieved by Rai using a patched grid and a similar number of grid points. The single deforming grid used in the present effort is shown in Fig. 2. As can be seen, this approach basically combines a rigid 'C' grid for the leading stator and a rigid 'H' grid for the following rotor with a deforming section between them. The primary advantage of this approach is the absence of internal boundaries such as that which occurs in overlaid or patched grids, and the consequent expected decrease in run time. The main disadvantage of the single deforming grid approach lies in the limitation as to how close the rotor and stator could be placed. Obviously, a small gap would increase the interaction in both the rotor and stator. However, it is estimated for practical modern compressor blade shapes, a gap of 25% axial chord could be calculated with this approach, and for turbine blades a gap of 40% axial chord could be considered. These are close to the lower limits of the gaps currently used in practice.

The second difference in the approach concerns the numerical method. The method of Rai is a multiple grid approach for the "thin shear layer" approximation to the Navier-Stokes equations, in which the calculation is performed on several grids which then are patched together or overlaid. The method used for each individual grid is a factored, iterative implicit technique which is an extension of the noniterative techniques of Ref. 18. In brief, for each time step, the technique solves the equations on each subgrid by an approximate factorization technique. However, an iteration at each time step is incorporated within the method. These additional iteration steps are used primarily to match the solutions at patched and overlaid boundaries. Although, use of the additional iteration increases run time, it does have the beneficial effect of decreasing splitting and linearization errors.

The approach used in the present effort solves the full time-dependent Navier-Stokes equations via a technique in which a single grid deforms to accommodate the relative motion. A single double sweep LBI procedure based upon the technique of Refs. 19 and 20 is used to advance the solution each time step. Although an iteration could be incorporated to reduce the splitting error and improve transient accuracy, previous experience (Ref. 21) indicates that at modest subsonic Mach numbers, $M \geq 0.35$, accurate time-dependent results can be obtained for airfoil type problems in this frequency regime. Furthermore, for many aircraft gas turbine applications, the limiting low Mach number of 0.35 for transient accuracy with the time step used here falls within the range of practical applications. The techniques of the present effort appear to be considerably more efficient in terms of computer run time for a cycle, and this represents a major advantage. However, vis-a-vis the patched grid approach, the technique is limited in terms of minimum gap.

ANALYSIS

Governing Equations

The equations used are the full ensemble-averaged time-dependent Navier-Stokes equations which can be written in vector form as

Continuity

$$\frac{\partial \rho}{\partial t} + \nabla \cdot \rho \vec{U} = 0 \tag{1}$$

Momentum

$$\frac{\partial \rho \vec{U}}{\partial t} + \nabla \cdot (\rho \vec{U}\vec{U}) = -\nabla P + \nabla \cdot (\overset{\rightarrow}{\overset{\rightarrow}{\pi}} + \overset{\rightarrow}{\overset{\rightarrow}{\pi}}^{T}) \tag{2}$$

Energy

$$\frac{\partial \rho h}{\partial t} + \nabla \cdot (\rho \vec{U} h) = -\nabla \cdot (\vec{Q} + \vec{Q}^{T}) + \frac{DP}{Dt} + \Phi + \rho\varepsilon \tag{3}$$

where ρ is density , $\vec{U}$ is velocity, P is pressure, $\overset{\rightarrow}{\overset{\rightarrow}{\pi}}$ is the molecular stress tensor, $\overset{\rightarrow}{\overset{\rightarrow}{\pi}}^{T}$ is the turbulent stress tensor, h is enthalpy, $\vec{Q}$ is the mean heat flux vector, $\vec{Q}^{T}$ is the turbulent heat flux vector, Φ is the mean flow dissipation rate and ε is the turbulence energy dissipation rate. If the flow is assumed as having a constant total temperature, the energy equation is replaced by

$$T_t = T + \frac{q^2}{2C_p} = \text{constant} \tag{4}$$

where T_t is the stagnation temperature, q is the magnitude of the velocity, and C_p is the specific heat at constant pressure. In the cases considered in this work, the total temperature has been assumed constant. This assumption was made solely to reduce computer run time, and the code has the capability to solve an energy equation, as has been demonstrated in Ref. 8.

It should be noted that for time-dependent flows such as the rotor-stator flow field, the constant total temperature assumption is an approximation. As discussed in Ref. 21, the analysis of Ref. 22 shows the effect of unsteady flow is proportional to the Mach number squared and the frequency. In terms of demonstration results, such as those presented here, at the Mach number and frequencies considered, the qualitative nature of the flow field should be correct. The effect of this total temperature constant assumption on quantitative results will require further investigation. In any case, future efforts can easily include an energy equation.

A number of terms appearing in equations (1-4) require definition. The stress tensor appearing in equation (4) is defined as

$$\overset{\ddagger}{\pi} = 2\mu\overset{\ddagger}{D} - \left(\frac{2}{3}\mu - K_B\right)\nabla\cdot\vec{U}\overset{\ddagger}{I} \tag{5}$$

where K_B is the bulk viscosity coefficient, $\overset{\ddagger}{I}$ is the identity tensor and $\overset{\ddagger}{D}$ is the deformation tensor, defined by:

$$\overset{\ddagger}{D} = \frac{1}{2}\left((\nabla\vec{U}) + (\nabla\vec{U})^T\right) \tag{6}$$

In addition, the turbulent stress tensor has been modeled using an isotropic eddy viscosity such that:

$$\overset{\ddagger}{\pi}_T = -\rho\overline{u'u'} = 2\mu_T\overset{\ddagger}{D} - \frac{2}{3}\left(\mu_T\nabla\cdot\vec{U}\right)\overset{\ddagger}{I} \tag{7}$$

where μ_T, the turbulent viscocity, is determined by a suitable turbulence model. Turbulence modeling is described in the next section.

Equation (3) contains a mean heat flux vector defined as follows:

$$\vec{Q} = -\kappa\nabla T \tag{8}$$

and a turbulent heat flux vector defined as:

$$\vec{Q}^T = -\kappa^T \nabla T \tag{9}$$

where κ and κ^T are the mean and turbulent thermal conductivities.

Also appearing in equation (8) is the mean flow dissipation term Φ.

$$\Phi = 2\mu \vec{\vec{D}} : \vec{\vec{D}} - \left(\frac{2}{3}\mu - K_B\right)(\nabla \cdot \vec{U})^2 \tag{10}$$

The equation of state for a perfect gas

$$P = \rho RT \tag{11}$$

where R is the gas constant, the caloric equation of state

$$e = C_v T \tag{12}$$

and definition of static enthalpy

$$h = C_p T \tag{13}$$

supplement the equations of motion.

In regard to molecular viscosity, thermal conductivity and bulk viscosity, the existing code sets bulk viscosity to zero and allows μ and κ to either be constant or have a Sutherland type law variation. The results presented here were obtained with μ constant and the total temperature assumption replacing the energy equation.

Dependent Variables and Coordinate Transformation

The governing equations, equations (1-2), are written in general vector form and, prior to their application to specific problems, it is necessary to decide upon both a set of dependent variables and a proper coordinate transformation. Based upon previous investigations (e.g., Ref. 6), the specific

scalar momentum equations to be solved are the x and y Cartesian momentum equations. The dependent variables chosen are the physical Cartesian velocities u and v and the density ρ.

The present application focuses upon two-dimensional time-dependent flows with the assumption of constant total temperature. Therefore, the remainder of the equation development will be within this framework. The equations are transformed from the Cartesian variables x, y to a set of general coordinates ξ, η where

$$\xi = \xi(x, y, t)$$

$$\eta = \eta(x, y, t) \tag{14}$$

$$\tau = t$$

The equations themselves can be expressed in either the so-called "strong conservation form"

$$\frac{\partial W/D}{\partial \tau} + \frac{\partial}{\partial \xi}\left(\frac{W\xi_t}{D} + \frac{F\xi_x}{D} + \frac{G\xi_y}{D}\right) + \frac{\partial}{\partial \eta}\left(\frac{W\eta_t}{D} + \frac{F\eta_x}{D} + \frac{G\eta_y}{D}\right)$$

$$= \frac{1}{Re}\frac{\partial}{\partial \xi}\left(\frac{F_1\xi_x}{D} + \frac{G_1\xi_y}{D}\right) + \frac{\partial}{\partial \eta}\left(\frac{F_1\eta_x}{D} + \frac{G_1\eta_y}{D}\right) \tag{15}$$

or the so-called "quasi-linear" or "chain rule conservation" form

$$\frac{\partial W}{\partial \tau} + \xi_t\frac{\partial W}{\partial \xi} + \xi_x\frac{\partial F}{\partial \xi} + \xi_y\frac{\partial G}{\partial \xi} + \eta_t\frac{\partial W}{\partial \eta} + \eta_x\frac{\partial F}{\partial \eta} + \eta_y\frac{\partial G}{\partial \eta}$$

$$= \frac{1}{Re}\left(\xi_x\frac{\partial F_1}{\partial \xi} + \eta_x\frac{\partial F_1}{\partial \eta} + \xi_y\frac{\partial G_1}{\partial \xi} + \eta_y\frac{\partial G_1}{\partial \eta}\right) \tag{16}$$

where

$$D = \xi_x \eta_y - \xi_y \eta_x \tag{17}$$

$$W = \begin{pmatrix} \rho \\ \rho u \\ \rho v \end{pmatrix}, \quad F = \begin{pmatrix} \rho u \\ \rho u^2 + p \\ \rho uv \end{pmatrix}, \quad G = \begin{pmatrix} \rho v \\ \rho uv \\ \rho v^2 + p \end{pmatrix} \quad F_1 = \begin{pmatrix} 0 \\ \tau_{xx} \\ \tau_{xy} \end{pmatrix} \quad G_1 = \begin{pmatrix} 0 \\ \tau_{xy} \\ \tau_{yy} \end{pmatrix}$$

The advantages of the two possible forms have been discussed in detail in Refs. 23-25. If the strong conservation form of the equations is to be used, then care must be taken to evaluate the metric data by a method which is consistent with a control volume approach (Refs. 23 and 24). Usually this requires numerical evaluation of the metric data <u>even</u> if an analytical functional relationship for the transformation is available. The analytical representation of the metric data, ξ_x, ξ_y, etc., when combined with the strong conservation form of the equations, leads to significant error for as straightforward a calculation as low Reynolds number flow about a circular cylinder (Ref. 23). The quasi-linear form of the equations is much less sensitive to the form of metric evaluation and gives good results for both numerical and analytical evaluations of the metric data. Furthermore, good results have been obtained with this approach by the present authors for a variety of steady state and time-dependent problems (e.g., Refs. 6, 8 and 21). Therefore, the set of equations represented by Eq. (16) was used in the present study.

It should be noted that the previous calculations were made with non-deforming coordinate grids. In the present stator-rotor application, most of the grid is non-deforming, however, a deforming region is present between the blades. Therefore, the use of the "quasi-linear" or "chain rule conservation" form with the deforming grid between blades is an item which may require further investigation.

The Turbulence Model

Although the code contains both a mixing length model and a two-equation turbulence model, and results have been obtained with both (e.g., Ref. 8), the present effort utilized a mixing length type model. The mixing length model assumes the existence of a mixing length, ℓ, and then relates an eddy

viscosity μ_T, to the mixing length by

$$\mu_T = \rho \ell^2 \left(\left(\frac{\partial u_i}{\partial x_j} + \frac{\partial u_j}{\partial x_i} \right) \frac{\partial u_i}{\partial x_j} \right)^{1/2} \tag{18}$$

For flow regions upstream of the leading edge where the flow is attached, the mixing length is determined by the usual boundary layer formulation

$$\ell = \kappa y D \qquad \ell \leq \ell_{max} \tag{19}$$

where κ is the von-Karman constant, D is a sublayer damping factor and ℓ_{max} is taken as 0.09 δ where δ is the boundary layer thickness. The damping factor, D, which has for the most part been utilized, is the van Driest damping factor

$$D = (1 - e^{-y^+/27}) \tag{20}$$

where y^+ is the dimensionless coordinate normal to the wall, yu_τ/ν.

When the mixing length formulation is used in a boundary layer environment, δ is usually taken as the location where $u/u_e = 0.99$. However, this definition assumes the existence of an outer portion of the flow where u_e is independent of distance from the wall, and assumes that the location where u_e becomes independent of distance from the wall marks the end of the viscous region. In a cascade Navier-Stokes calculation no such clear flow division occurs. Therefore, the boundary layer thickness, δ, is set by first determining u_{max}, the maximum velocity at each given streamwise station, and then setting δ by

$$\delta = 2.0 y_{(u/u_{max} = \kappa_1)} \tag{21}$$

i.e., δ is taken as twice the distance from the wall to the location where $u/u_{max} = k_1$. In the present calculation k_1 was set to 0.90.

In the wake region, the free turbulent shear flow model of Rudy and Bushnell (Ref. 26) is used. In brief, this model evaluated two length scales, δ_I and δ_{II}

$$\delta_I = 1.2 \times (y_{.95} - y_{CL}) + (x - x_{TE}) \tan 8° \qquad (22)$$

$$\delta_{II} = 2 \times 1.2 \times (y_{.95} - y_{CL})$$

where $y_{.95}$ is the location where the velocity is 95 percent of the free-stream velocity, y_{CL} is the centerline location and x_{TE} is the trailing edge location. This model was developed for symmetric wakes and was modified for the present application by setting

$$(y_{.95} - y_{CL}) = 0.5 \times (y^+_{.95} - y^-_{.95}) \qquad (23)$$

where $y^+_{.95}$ and $y^-_{.95}$ represent the upper and lower locations where the wake velocity reaches 95% of the freestream velocity. Following Ref. 26, the mixing length, ℓ, was taken as

$$\ell = 0.07 \times \text{MIN} (\delta_I, \delta_{II}) \qquad (24)$$

In some preliminary unpublished work at SRA, this model has given good agreement with data for the near wake region of a single row cascade. In the stage problem examined here, the wake of the leading blade impinges upon the trailing blade, and it is not clear how well the details of this can be simulated with a mixing length type model. However, in this initial effort, a mixing length model should give reasonable qualitative results, with a more sophisticated model being considered for future efforts.

Boundary Conditions

The authors' experience in solving Navier-Stokes equations has indicated the important role boundary conditions play in determining accurate solutions and rapid numerical convergence. The present approach follows the tack of Briley and McDonald (Ref. 27). In brief, this approach sets total pressure and flow angle at the upstream inflow boundary and static pressure at the downstream outflow boundary. These represent the physical boundary

conditions for the governing set of differential equations. In addition, the density derivative is set to zero at the upstream boundary, and second derivatives of both velocity components are set to zero at the downstream boundary. On the blade surface, no slip conditions are applied. These are applied with sublayer resolution; wall functions are not used, as the first point off the wall is generally within the sublayer. In addition, the wall normal pressure gradient is set to zero. Finally, periodic conditions are applied in an implicit manner on the periodic line.

One item of interest in regard to boundary conditions concerns the downstream constant pressure boundary. Since this is a reflecting boundary condition, it was decided to explore possible non-reflecting boundary conditions. After surveying the literature, a condition based upon the work of Rudy and Strikwerda (Ref. 28), and Engquist and Majda (Ref. 29) was incorporated into the code upon option. Cases were run for a single blade row, however, this did not appear to give any advantage in convergence properties over the constant pressure boundary. In addition, the final results were nearly identical to those obtained with the constant pressure boundary condition.

Numerical Procedure

The numerical procedure used to solve the governing equations is a consistently split linearized block implicit (LBI) scheme originally developed by Briley and McDonald (Ref. 19). A conceptually similar scheme has been developed for two-dimensional MHD problems by Lindemuth and Killeen (Ref. 30). The procedure is discussed in detail in Refs. 19 and 20. The method can be briefly outlined as follows: the governing equations are replaced by an implicit finite difference approximation, optionally a backward difference or Crank-Nicolson scheme. Terms involving nonlinearities at the implicit time level are linearized by Taylor expansion in time about the solution at the known time level, and spatial difference approximations are introduced. The result is a system of multidimensional coupled (but linear) difference equations for the dependent variables at the unknown or implicit time level. To solve these difference equations, the Douglas-Gunn (Ref. 31) procedure for generating alternating direction implicit (ADI) schemes as perturbations of fundamental implicit difference schemes is introduced, in its natural extension, to systems of coupled linear difference

equations having narrow-block banded matrix structures which can be solved efficiently by standard block-elimination methods.

The method centers around the use of a formal linearization technique adapted for the integration of initial-value problems. The linearization technique, which requires an implicit solution procedure, permits the solution of coupled nonlinear equations in one space dimension (to the requisite degree of accuracy) by a one-step noniterative scheme. Since no iteration is required to compute the solution for a single time step, and since only moderate effort is required for solution of the implicit difference equations, the method is computationally efficient; this efficiency is retained for multidimensional problems by using what might be termed block ADI techniques. The method is also economical in terms of computer storage, and in its present form requires only two time levels of storage for each dependent variable. Furthermore, the block ADI technique reduces multidimensional problems to sequences of calculations which are one-dimensional, in the sense that easily solved narrow block-banded matrices associated with one-dimensional rows of grid points are produced.

Artificial Dissipation

The final item to be considered concerns the use of articifial dissipation. Since the calculations were at high Reynolds numbers typical of normal turbomachinery applications, it was necessary to add "articifial dissipation" terms to suppress central difference spatial oscillations. Such "artificial dissipation" could be added via the spatial differencing formulation (e.g., one-sided difference approximations for first derivatives) or by explicitly adding an additional dissipative type term. The present authors favor the latter approach, since when an additional term is explicitly added, the physical approximation being made is usually clearer than when dissipative mechanisms are contained within numerical truncation errors, and further, explicit addition of an artificial dissipation term allows greater control over the amount of nonphysical dissipation being added. Obviously, the most desirable technique would add only enough dissipative mechanism to suppress oscillations without deteriorating solution accuracy. Various methods of adding artificial dissipation were investigated in Ref. 32, and these were evaluated in the context of a model one-dimensional problem containing a shock with a known analytic solution (one-dimensional flow with heat

transfer). The methods considered included second-order dissipation, fourth-order dissipation and pressure dissipation techniques.

As a result of this investigation, it was concluded that a second-order anisotropic artificial dissipation formulation suppressed spatial oscillations without impacting adversely on accuracy, and could be used to capture shocks successfully. In this formulation the terms

$$\frac{\partial}{\partial x}\left(\rho^{n-1} d_x \quad \partial\phi/\partial x\right)$$

are added to the governing equations where ϕ = u, v and ρ for the x-momentum, y-momentum, and continuity equations, respectively. The exponent, n, is zero for the continuity equation and unity for the momenta equations. The dissipation coefficient, d_x, is determined as follows. The general equation has an x-direction convective term of the form $a\partial\phi/\partial x$ and an x-direction diffusion term of the form $\partial(b\partial\phi/\partial x)/\partial x$. The diffusive term is expanded

$$\partial(b\partial\phi/\partial x)/\partial x = b\partial^2\phi/\partial x^2 + \partial b/\partial x\,\partial\phi/\partial x \qquad (25)$$

and then a local cell Reynolds number $Re_{\Delta x}$ is defined for the x-direction by

$$Re_{\Delta x} = \left|a - \partial b/\partial x\right| \Delta x/b \qquad (26)$$

where b is the total effective viscosity, including both laminar and turbulent contributions, and Δx is the grid spacing. The dissipation coefficient d_x is nonnegative and is chosen as the larger of zero and the local quantity $\mu_e(\sigma_x Re_{\Delta x} - 1)$. The dissipation parameter σ_x is a specified constant and represents the inverse of the cell Reynolds number below which no artificial dissipation is added. The dissipation coefficient, d_y, is evaluated in an analogous manner and is based on the local cell Reynolds number $Re_{\Delta y}$, grid spacing Δy for the y-direction and the specified parameter σ_y.

The question naturally arises as to the value to be used for σ_x and σ_y. Based upon a wide variety of experience (e.g., Refs. 6, 8, 21, 32), it has been concluded that values of σ_x and σ_y of 0.05 are sufficient to suppress spurious oscillations, but do not lead to non-physical damping of

the mean flow. In some cases where gradients are large and grids relatively coarse in terms of the change of dependent variable from point to point; for example, the leading edge stagnation region; it may be necessary to increase the streamwise dissipation to 0.5 locally. However, the normal dissipation is held at 0.05.

RESULTS

Assessment of Time-Accuracy

The Navier-Stokes cascade code which is used in the present stator-rotor simulation has been successfully exercised for a variety of steady state cascade flow fields (e.g., Refs. 6, 8, 23), however, an assessment was still required as to the time accurate nature of the procedure. In this regard, two calculations are relevant. The first, an oscillating airfoil calculation, was performed by SRA under contract to NASA Langley Research Center as part of a dynamic stall analysis (Ref. 21). The second case considered was performed under the present effort. The case was a 25.5% thick Joukowski airfoil entering a gust in which the vertical velocity is 0.25 times the freestream velocity.

In regard to the oscillating airfoil calculation, the case considered was that of an NACA 0012 airfoil oscillating sinusoidally in pitch in a stream with a Reynolds number based on chord of 2.08×10^6 and a Mach number of 0.30. The airfoil oscillated between 4° and 20° with a dimensionless frequency of 0.125. The case corresponds to Data RUN 51.005 of the data of St. Hilaire and Carta (Refs. 33 and 34). Although this calculation represents an isolated airfoil rather than a cascade, it was made with a code essentially identical to the cascade deck used here with boundary conditions appropriate to the isolated airfoil applied.

Comparisons between calculated and measured surface pressure coefficients are shown in Figs. 3-10. Three comparisons during the upstroke are shown in Figs. 3 and 4. As can be seen, the agreement is good. The data was reconstructed from the Fourier coefficient given by St. Hilaire and Carta (NASA CR-165927). The third measured data point on the pressure surface ($x/c \approx .066$) gave very erratic results and was not plotted for most of the comparisons. The excellent comparisons shown in Figs. 3 and 4 give evidence to the time-accurate calculation for the surface pressure. Figure 5 presents a comparison at $\alpha = 17.7°$, $\dot{\alpha} > 0$. This is near the incidence where stall would first be inferred from the lift and moment curves. The figure shows some discrepancy between predicted and measured values as the data presents some evidence of a vortex being shed on the suction surface leading edge. The discrepancy increases in Fig. 6 where the data clearly indicates stall.

The calculated plateau on the suction surface, x/c ≈ .15, seems to indicate a vortex being initiated. Furthermore, the calculated maximum suction peak at $\alpha = 19.5°$, Fig. 6, is considerably less than that at $\alpha = 17.7°$, Fig. 5. Based upon the plateau and the drop in suction peak, the calculated distribution at 19.5° appears to be beginning the stall process. The data at 19.5° is presented with the calculation at $\alpha = 19.9°$, $\dot{\alpha} > 0$ in Fig. 7. Although these are at different values of α, they represent pressure distributions at approximately the same incremental time after stall is initiated; the distributions are remarkably similar. Comparisons over the downstroke are given in Figs. 8-10. Obviously, the basic trends are in agreement, as a strong qualitative comparison is shown between the calculation and the measured data. The results of this calculation, particularly prior to stall, Figs. 3-5, indicate the time-accuracy of the procedure, at least as far as surface pressure is concerned. Although the reduced frequency for the oscillating airfoil calculation is approximately an order of magnitude less than that found in a typical rotor-stator interaction, the accurate and efficient calculation of transients is more demanding from a numerical point of view for low reduced frequencies than for high reduced frequencies.

The second case considered was performed under the present effort. The case was a 25.5% thick Joukowski airfoil entering a gust in which the vertical velocity is 0.25 times the freestream velocity. This case was also calculated by Giesing via an inviscid analysis (Ref. 35) and although viscous effects are present in the present analysis, it is expected that the calculated pressure gradients should be in reasonable agreement if little or no separation occurs. Calculated surface pressure distributions from both techniques are presented in Figs. 11-14, where T indicates the location of the gust relative to the airfoil leading edge. As can be seen, the two calculations are in good agreement. The major discrepancies are the appearance of surface pressure discontinuities in the inviscid solution which are not found in the viscous solution, such as at x/c = .25 in Fig. 12. However, this is the expected result of viscous effects. This comparison along with the dynamic stall calculations of Ref. 21 serve to confirm the time-accuracy capability of the cascade code in prediction of surface pressure for these frequencies, geometries, Reynolds numbers and Mach numbers.

H-Grid Assessment

The stator system to be used consists of a 'C' grid coordinate system for the leading stator blade followed by an 'H' grid system for the rotor; these two grids are joined by a deforming section, as shown in Fig. 2. Although considerable work had been performed in a 'C' grid context, the existing coordinate system had not been exercised for an 'H' grid. Therefore, prior to performing a stage calculation, it was decided to perform a single blade row calculation with an 'H' grid coordinate system. The case originally chosen was flow about a 25.5% thick Joukowski airfoil at zero incidence. This case was chosen since the relatively thick leading edge region presented a relatively difficult test case for the 'H' grid. In addition, the symmetric cascade should give a symmetric flow field which would aid in verifying the code. The 'H' grid used is shown in Fig. 15. A comparison between pressure distributions as calculated by the 'H' and 'C' grids is shown in Fig. 16. These were performed for turbulent flow and showed very good correspondence. The 'C' grid capability has been assessed in a variety of comparisons (e.g., Refs. 6, 8, 21, 23) and therefore, this serves to confirm the 'H' grid capability. In particular, it should be noted that the stagnation point pressure coefficient with the 'H' grid was approximately 0.96. This is at the coordinate singularity, and represents a demanding computation for the 'H' grid. The computed C_p of 0.96 should be regarded as quite good. In addition, the calculation proved to be symmetric, as indicated by the contour plot shown in Fig. 17.

Stator-Rotor Calculation

The final case of interest is the stator-rotor stage calculation, which is the focus of the present effort. The case chosen for calculation was a stage formed from two sets of compressor blade profiles of Hobbs, Wagner, Dannenhoffer and Dring (Ref. 5). This blade shape has been previously considered as a cascade at SRA, and numerical simulations of the flow in this cascade had shown good correspondence when compared against the experimental data (Ref. 6). The calculation was run for a stage in which the Reynolds number at inflow was 6.8×10^5; the inflow Mach number was 0.47. The grid used consisted of a constructive 'C'-grid for the upstream stator, a constructive 'H' grid for the downstream rotor and a taut spline blending

region between the two. As previously discussed, the calculation set upstream total pressure and flow angle and downstream static pressure. The upstream flow angle was set at a value of 38° and the upstream total to downstream static pressure set at a ratio of 1.0807. The rotor wheel speed was set at 52 per cent of the velocity upstream of the stator leading to the incidence on the rotor in a frame tied to the rotor being approximately 38°. A figure showing these velocities is presented in Fig. 18.

The calculation was run on a very highly resolved grid. The first point off the blade was approximately $3x10^{-5}$ chords from the blade. High resolution was obtained in both the stator and rotor leading edge regions. The blade spacing between rotor and stator was 0.5 axial chords; the spacing between adjacent rotor blades (or stator blades) was 0.72 axial chords. A computer plot of the grid is shown at three different times in Fig. 19. As can be seen, the grid is a rigid 'C' grid in the vicinity of the stator; i.e. upstream of point A, and a rigid 'H' grid in the vicinity of the rotor; i.e. downstream of point B. Between A and B the grid deforms. A cycle begins with the grid in the position of the lower figure, T = 8.0. The calculation proceeds with the grid moving until the position at T = 9.0 is reached. This represents a cycle; the grid is then moved back to the position at T = 8.0, the results in the deformed region are interpolated, and the calculation then continues.

The calculation required approximately five cycles to reach a condition of cyclic periodicity in the solution. Each cycle required 100 time steps and approximately 4 CPU minutes of CRAY run time. The code being used is a partially vectorized code; a more recent version of this same code is fully vectorized and runs twice as fast as that used here. Therefore, it is reasonable to expect run times of 2 CPU CRAY minutes per cycle for 7500 grid points to be attainable. Plots of Mach number contours for this configuration at three different time levels are shown in Figs. 20 and 21. During this calculation, minor changes were made in the turbulence model, as well as in the leading edge region artificial dissipation. Therefore, this does not represent nine cycles of calculation. As previously stated, a reasonably periodic solution is obtained within five cycles. For the current test case, the major interactive effect is on the trailing blade. This can be seen clearly in the Mach number contours where the flow field changes significantly between T = N and T = N+0.5. In the latter case, the stator

wake impinges directly upon the rotor leading edge. In the former case, it lies within the passages. No major effect is noted on the flow in the upstream blade passage for this blade streamwise spacing. The change in static pressure contours through the cycle appears less dramatic than the change in Mach number coutours. However, significant changes do occur particularly in the leading edge regions when viewed in terms of pressure coefficient perturbation.

A plot of the 'baseline' rotor surface pressure coefficient is shown in Fig. 22. This represents the surface pressure at a time when the rotor leading edge location is midway between the stator trailing edges. It should be noted that this should be approximately the minimum interference configuration. It does not represent a result time-averaged over the cycle. The rotor leading edge stagnation point pressure coefficient is considerably greater than unity ($\approx$1.33) due to the work being performed on the fluid by the moving blade. The pressure coefficient was smooth throughout the flow except in the immediate vicinity of the leading edge ($x/c<.001$) where some oscillations occurred. In any case, it is confined to a very small region of the flow.

Pressure coefficient perturbations relative to the base case are presented in Figs. 22-28. In these figures, the relative positions of the rotor leading edge and stator trailing edge are noted on the left side of the figures. It should be noted that surface pressure perturbations are expected to occur as the rotor passes through the nonuniform exit flow field generated by the stator. As the rotor passes through the stator wake it experiences (i) a decrease in flow stagnation pressure due to losses in the wake and (ii) an increase in flow incidence due to a decrease in axial velocity. It is estimated that the flow incidence changes from approximately 32° from horizontal when the rotor is between stator blades, to approximately 38° when the rotor is in the stator wake. In addition, when the rotor is in the stator wake, it experiences an oncoming shear flow which will affect the blade loading.

The results of Figs. 23-28 show the surface pressure perturbation as the rotor passes through the cycle. The base case shown in Fig. 22 gives the pressure distribution when the rotor is between the stator blades. At this location, the incoming flow angle relative to the rotor is at its minimum angle to the horizontal. As time progresses, the rotor moves into the wake

and the relative flow angle increases, giving an increased pressure on the leading edge region pressure surface and a decreased pressure on the leading edge region suction surface. This becomes most pronounced at T = 8.59 to 8.67, as shown in Figs. 26 and 27. During this portion of the cycle considerable additional leading edge loading occurs with ΔC_p being approximately 0.4. At all times the major loading perturbations are confined to the leading edge region, X/C<0.2. As the flow proceeds into the passage, X/C>0.2, the flow basically behaves as a channel flow and the surface pressure distribution is relatively insensitive to the incoming flow angle. The major effect being in the leading edge region has serious implications in terms of time-dependent pitching moment and possible structural consequences.

Although the major effect is in the rotor leading edge, there is a smaller effect over the entire blade. As shown in Figs. 23-28, both the pressure and suction surfaces show a pressure perturbation over the entire blade chord. Since this perturbation becomes very small at T ≈ 9.0, Fig. 28, it does not represent a significant aperiodicity still present in the solution. Downstream of the leading edge the perturbation is more pronounced on the suction surface, reaching a maximum perturbation C_p of -0.025.

The perturbation flow field in the trailing rotor blade was considerably stronger than that observed on the stator. However, some relatively small effects were noted on the stator. For example, the maximum suction peak on the stator ranged from -0.86 to -0.81, giving a ΔCp of approximately 0.05, with the highest value, -0.81, occurring when the trailing blade was approximately aligned with the leading blade. The trailing edge pressure coefficient ranged from 0.34 to 0.37, with the highest values again being when the stator trailing edge and rotor leading edge were approximately aligned. These results indicate a maximum interaction effect occurs on the leading stator blade when the blades are nearly aligned, and minimum interaction occurs when the rotor is between stators. However, it should be noted that these stator perturbations are relatively small.

In regard to data comparison, no data exists for this specific case. However, the data of Fleeter, Jay and Bennett (Ref. 36) can be used for guidance. This data was taken on a rotor/stator configuration with the rotor being the leading blade. The gap was approximately 0.4 axial chords. In general, this data shows the major perturbation, C_p, to be confined to the

leading edge region of the trailing blade. When normalized by the incoming dynamic head, the leading edge perturbation was approximately 0.10 to 0.30 over a range of flow conditions. This is the same order found in the present simulations. As in the present numerical flow simulation, although some perturbation was found downstream of the leading edge, it was considerably less than at the leading edge. This again is consistent with the results obtained here.

CONCLUSIONS AND RECOMMENDATIONS

The present effort has led to the development of a numerical procedure of the stage flow field based upon solution of the Navier-Stokes equations. The specific case considered is the basic case in which two-dimensional flow and equal rotor and stator pitch are assumed. The procedure developed is capable of obtaining periodic solutions for a grid of 7500 points within ten CPU minutes of Cray run time. This represents a very efficient technique which will permit runs of this type on a regular basis, and which will allow extension to either three dimensions or to stages in which rotor and stator have unequal pitch and to multiple stages.

The results obtained show the qualitatively expected features. Periodicity was obtained essentially within five cycles. The major effect of the interaction to the specific case considered appeared in the leading edge region of the downstream rotor blade. Significant perturbation pressures were noted, $\Delta Cp \approx 0.4$, which has major implications regarding unsteady loading and unsteady fluid structure interaction. The concentration of the interaction effect in the leading edge has particular significance in regard to unsteady pitching moment. Although less significant, unsteady effects were noted over the aft portion of the trailing blade, as well as over the entire leading blade.

Possible extensions of this work fall into three natural paths. Under the first additional two-dimensional, equal pitch calculations would be made and the results investigated with particular emphasis on the flow physics and possible structural implications of unsteady loading. The second path would consider three-dimensional flow in a stage. This would allow inclusion of the various vortices generated in the three-dimensional passage. Since the three-dimensional calculation is expected to require sixty times the computer resources as the two-dimensional, an efficient two-dimensional analysis is imperative as a base. The analysis developed under the present effort is very efficient and therefore would form a suitable base in meeting these goals. The third option is extension to the case of unequal rotor and stator pitch. Again, for this to be practical, an efficient base deck is key. Finally, a more long-term goal would be development of a two-dimensional multi-stage analysis based upon this approach.

REFERENCES

1. Dring, R.P., Joslyn, H.D. and Hardin, L.W.: An Investigation of Axial Compressor Rotor Aerodynamics, ASME Journal of Engineering for Power, Vol. 104, 1982.

2. Wagner, J.H., Dring, R.P. and Joslyn, H.D.: Inlet Boundary Layer Effects in an Axial Compressor Rotor, Part I - Blade-to-Blade Effects, ASME Paper 84-GT-84, 1984.

3. Joslyn, H.D. and Dring, R.P.: Axial Compressor Stator Aerodynamics, ASME Paper 84-GT-90,, 1984.

4. Shreeve, R.P. and Neuhoff, F.: Measurements of the Flow from a High Speed Compressor Rotor Using a Dual Probe Digital Sampling Technique. ASME ASME Journal of Engineering for Gas Turbine and Power, Vol. 106, 1984, pp. 366-375.

5. Hobbs, D.E., Wagner, J.H., Dannenhoffer, J.F., and Dring, R.P.: Experimental Investigation of Compressor Cascade Wakes. ASME Paper 82-GT-299, 1982.

6. Shamroth, S.J., McDonald, H. and Briley, W.R.: Prediction of Cascade Flow Fields Using the Averaged Navier-Stokes Equations, ASME Journal of Engineering for Gas Turbines and Power, Vol. 106, No. 2, April 1984, pp. 383-390.

7. Hah, C.: A Navier-Stokes Analysis of Three-Dimensional Turbulent Flows Inside Turbine Blade Rows at Design and Off Design Conditions, ASME Journal of Engineering for Gas Turbines and Power, Vol. 106, No. 2, April 1984, pp. 421-429; Paper No. 83-GT-40.

8. Weinberg, B.C., Yang, R.-J., McDonald, H. and Shamroth, S.J.: Calculation of Two- and Three-Dimensional Transonic Cascade Flow Using the Navier-Stokes Equations, ASME Journal of Engineering for Gas Turbines and Power, Vol. 108, No. 1, pp. 93-102.

9. Schafer, O., Fruhauf, H.H., Bauer, B. and Guggolz, M.: Application of A Navier-Stokes Analysis to Flows Through Plane Cascades. ASME Journal of Engineering for Gas Turbine and Power, Vol. 108, 1986.

10. Dawes, W.N.: Computation of Off-Design Flows in a Transonic Compressor Rotor. ASME Journal of Engineering for Gas Turbines and Power, Vol. 108, 1986.

11. Fleeter, S., Jay, R.L. and Bennett, W.A.: Compressor Stator Time-Variant Aerodynamic Response to Upstream Rotor Wakes, EDR 9005, Detroit Diesel Allison Contractor Report on Contract F44620-74-C-0065, November 1976.

12. Fleeter, S., Jay, R.L. and Bennett, W.A.: The Effect of Rotor-Stator Axial Spacing on the Time-Variant Aerodynamic Response of a Compressor Stator, EDR 9379, Detroit Diesel Allison Contractor Report on Contract F49620-77-C-0024, December 1977.

13. Jay, R.L. and Bennett, W.A.: The Effects of Solidity, Interblade Phase Angle and Reduced Frequency on the Time-Variant Aerodynamic Response of a Compressor Stator, EDR 10339, Detroit Diesel Allison Contractor Report on Contract F49629-78-C-0070, June 1980.

14. Jay, R.L. and Bettner, J.L.: Aerodynamically Induced Vibration, EDR 10840, Detroit Diesel Allison Contractor Report on Contract F49620-80-C-0078, September 1981.

15. Dring, R.P., Joslyn, H.D., Hardin, L.W. and Wagner, J.H.: Turbine Rotor-Stator Interaction, ASME Journal of Engineering for Power, Vol. 104, 1982, pp. 729-742.

16. Rai, M.M.: Navier-Stokes Simulation of Rotor-Stator Interactions Using Patched and Overlaid Grids, AIAA Paper 85-15-19, 1985.

17. Stephens, H.E. and Hobbs, D.E.: Design and Performance of Supercritical Airfoils for Axial Flow Compressors, Pratt and Whitney Aircraft Report FR11455, 1979.

18. Beam, R.M. and Warming, R.F.: An Implicit Factored Scheme for the Compressible Navier-Stokes Equations. Albuquerque, New Mexico, June 27-28, 1977.

19. Briley, W.R. and McDonald, H.: Solution of the Multidimensional Compressible Navier-Stokes Equations by a Generalized Implicit Method, Journal of Computational Physics, Vol. 244, 1977.

20. Briley, W.R. and McDonald, H.: On the Structure and Use of Linearized Block Implicit Schemes, Journal of Computational Physics, Vol. 13, 1973.

21. Shamroth, S.J.: Calculation of Steady and Unsteady Airfoil Flow via the Navier-Stokes Equations. NASA CR-3899, 1985. (Also AIAA Paper 84-525).

22. Briley, W.R., McDonald, H. and Shamroth, S.J.: A Low Mach Number Euler Formulation and Application to Time Iterative LBI Schemes. AIAA Journal, Vol. 21, 1983.

23. Shamroth, S.J. and Gibeling, H.: Navier-Stokes Solution of the Turbulent Flowfield About an Isolated Airfoil. AIAA Journal, Vol. 18, 1980, pp. 1409-1410.

24. Thomas, P.D. and Lombard, C.K.: Geometric Conservation Law and Its Application to Flow Computations on Moving Grids. AIAA Journal, Vol. 17, 1979, pp. 1030-1037.

25. Hindman, R.G.: Generalized Coordinate Forms of Governing Fluid Equations and Associated Geometrically Induced Errors. AIAA Journal, 20, October 1982, pp. 1359-1367.

26. Rudy, D.H. and Bushnell, D.M.: A Rational Approach to the Use of Prandtl's Mixing Length Model in Free Turbulent Shear Flows - Conference on Free Turbulent Shear Flows. NASA Langley Research Center, NASA SP-321, 1973.

27. Briley, W.R. and McDonald, H.: Computation of Three-Dimensional Horseshoe Vortex Flow Using the Navier-Stokes Equations. Seventh International Conference on Numerical Methods in Fluid Dynamics, 1980.

28. Rudy, D.H. and Strihwerda, H.C.: A Nonreflecting Outflow Boundary Condition for Subsonic Navier-Stokes Calculations. Journal of Computational Physics. Vol. 36, 1986.

29. Engquest, B. and Majda, A.: Absorbing Boundary Conditions for Numerical Simulation of Waves. Mathematics of Computation, Vol. 31, 1977.

30. Lindemuth, L.. and Killeen, J..: Alternating Direction Implicit Techniques for Two-Dimensional Magnetohydrodynamic Calculations. Journal of Computational Physics, Vol. 13, 1979, pp. 181-208.

31. Douglas, J. and Gunn, J.E.: A General Formulation of Alternating Direction Methods. Numerische Math., Vol. 6, 1964, pp. 428-453.

32. Shamroth, S.J., McDonald, H., and Briley, W.R.: A Navier-Stokes Solution for Transonic Flow Through a Cascade. SRA Report 81-920007-F, 1982.

33. St. Hilaire, A.O. and Carta, F.O.: Analysis of Unswept and Swept Wing Chordwise Pressure Data from an Oscillating NACA 0012 Airfoil Experiment, Vol. I - Technical Report, NASA CR-3567, 1983.

34. St. Hilaire, A.O. and Carta, F.O.: Analysis of Unswept and Swept Wing Chordwise Pressure Data from an Oscillating NACA 0012 Airfoil Experiment, Vol. II - Data Report, NASA CR-165927, 1983.

35. Giesing, J.P.: Nonlinear, Two-Dimensional Unsteady Potential Flow with Lift, AIAA Paper 66-968, 1966.

36. Fleeter, S., Jay, R.L. and Bennett, W.A.: Compressor Stator Time Variant Aerodynamic Response to Upstream Rotor Wakes. Detroit Deisel Allison Report EDR 9005A, 1976.

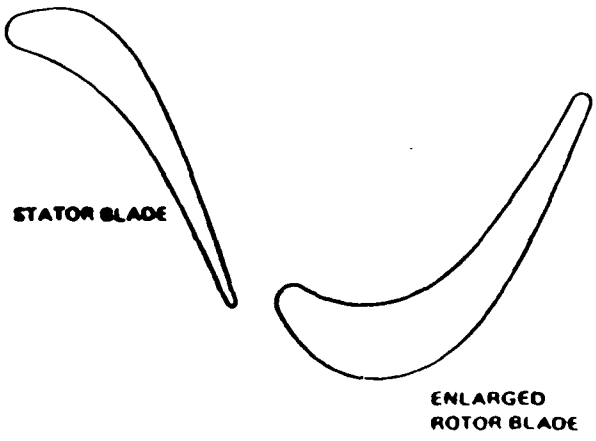

Figure 1a. Modified rotor - stator geometry.

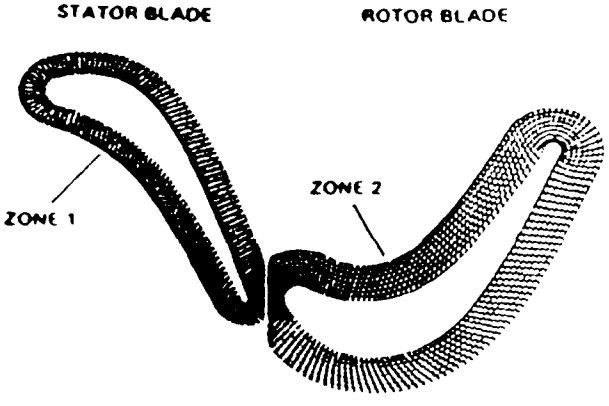

Figure 1b. "O"- type grids for zones 1 and 2.

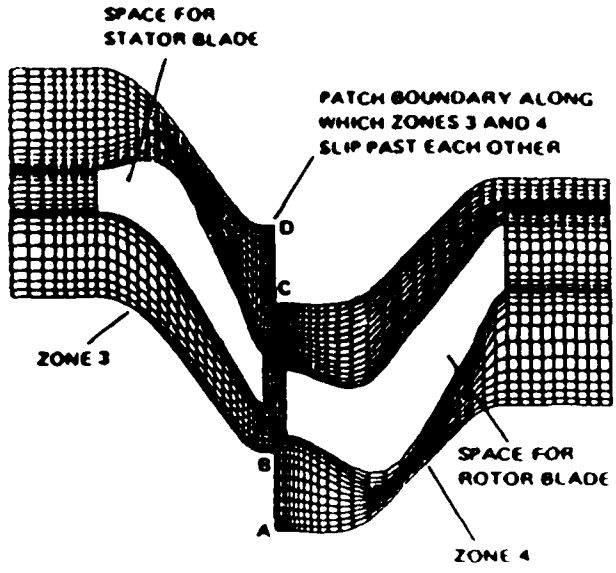

Figure 1c. Algebraically generated grids for zones 3.

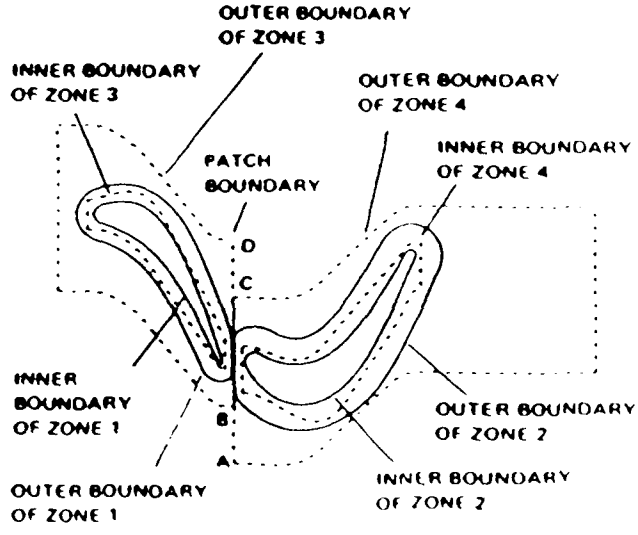

Figure 1d. Zoning of the rotor - stator problem showing patch and overlay boundaries.

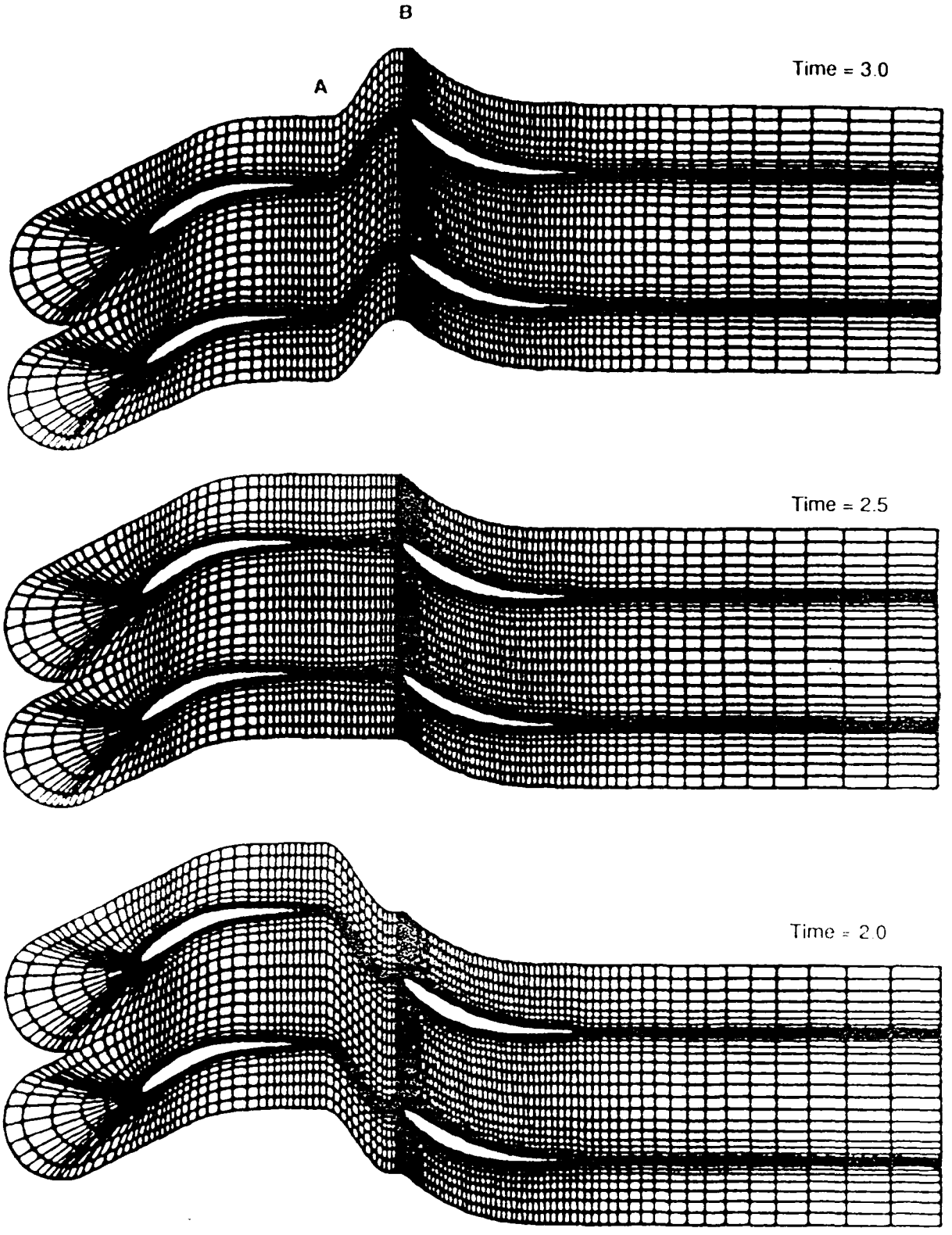

Figure 2 Rotor - stator coordinate system for the Stephens - Hobbs Cascade

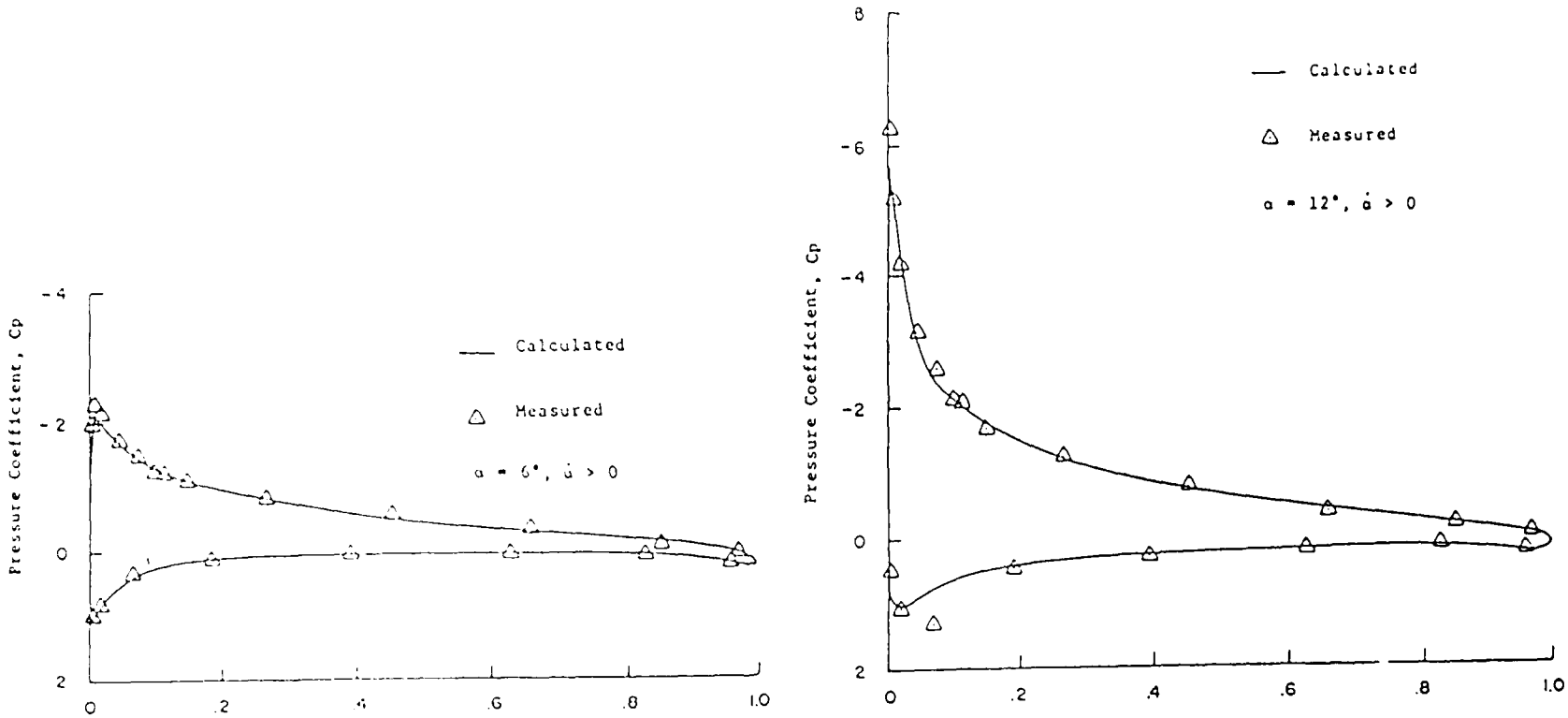

Figure 3. Pressure coefficient comparison - NACA 0012 airfoil.

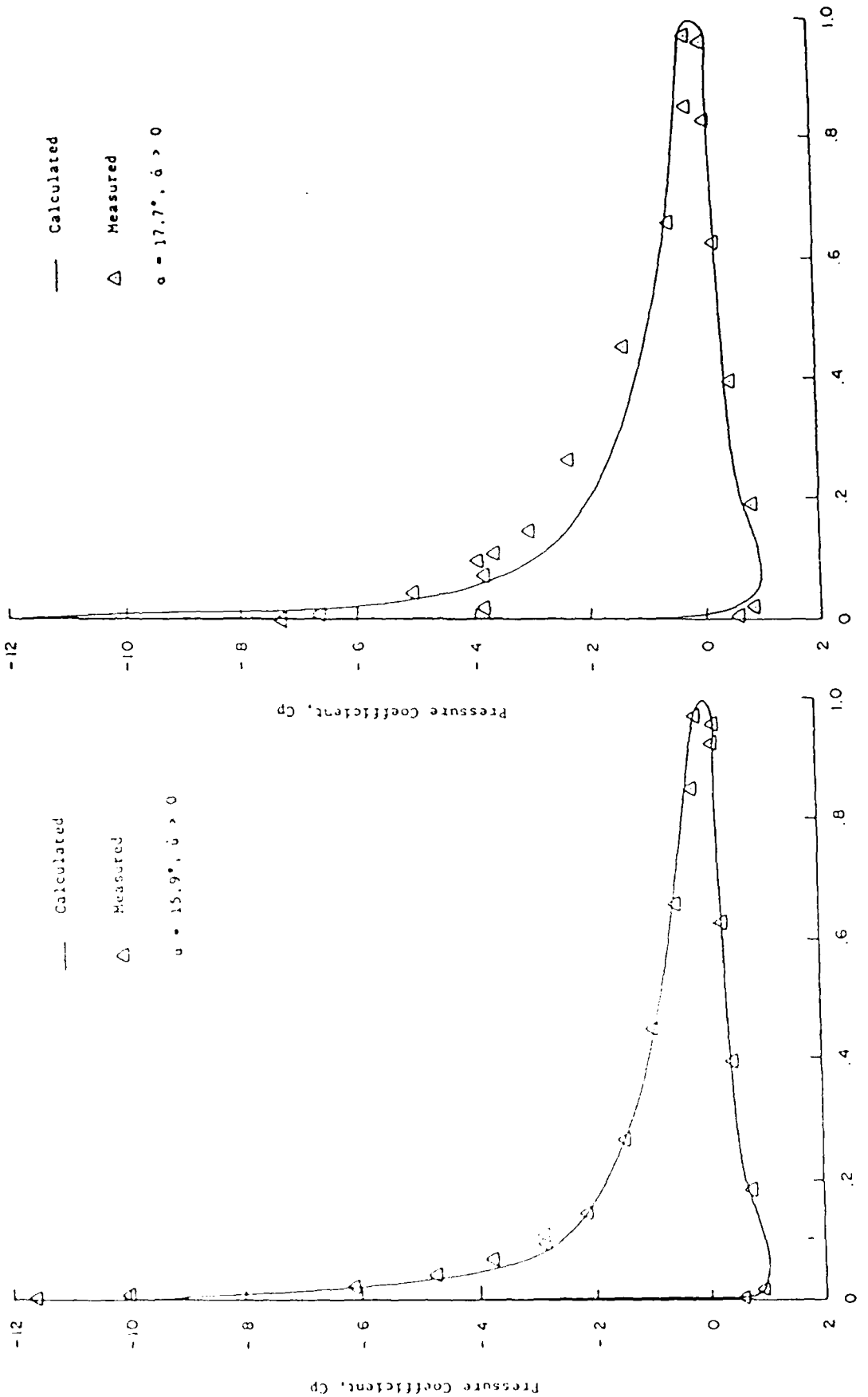

Figure 5.

Figure 4.

Pressure coefficient comparison - NACA 0012 airfoil.

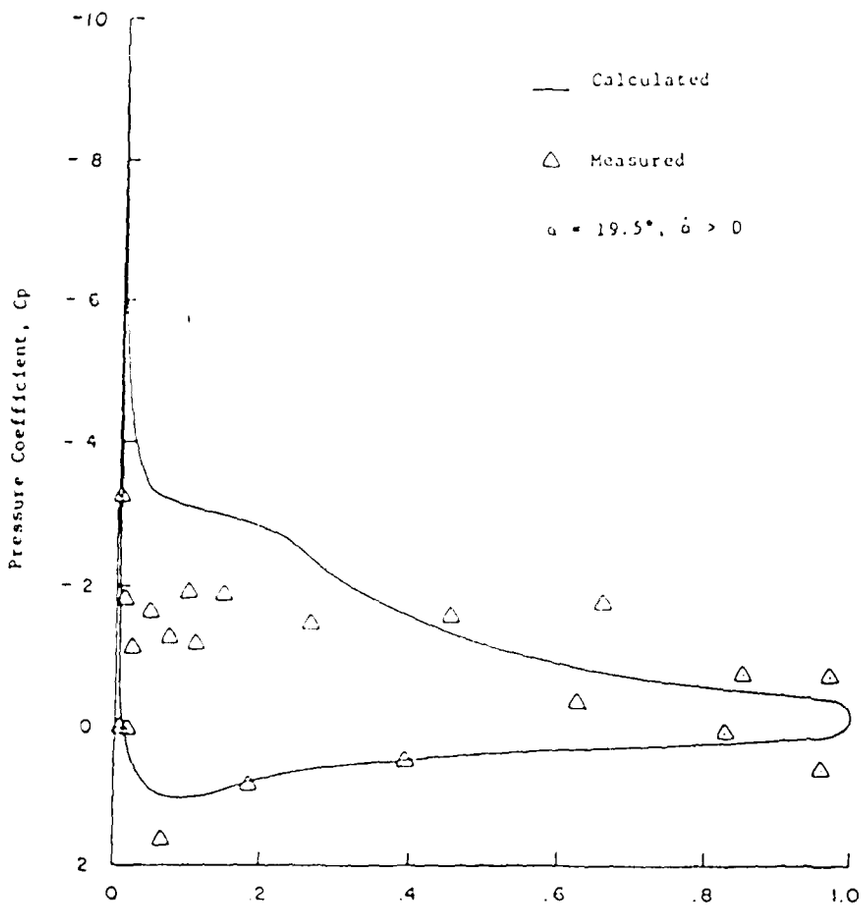

Figure 6.

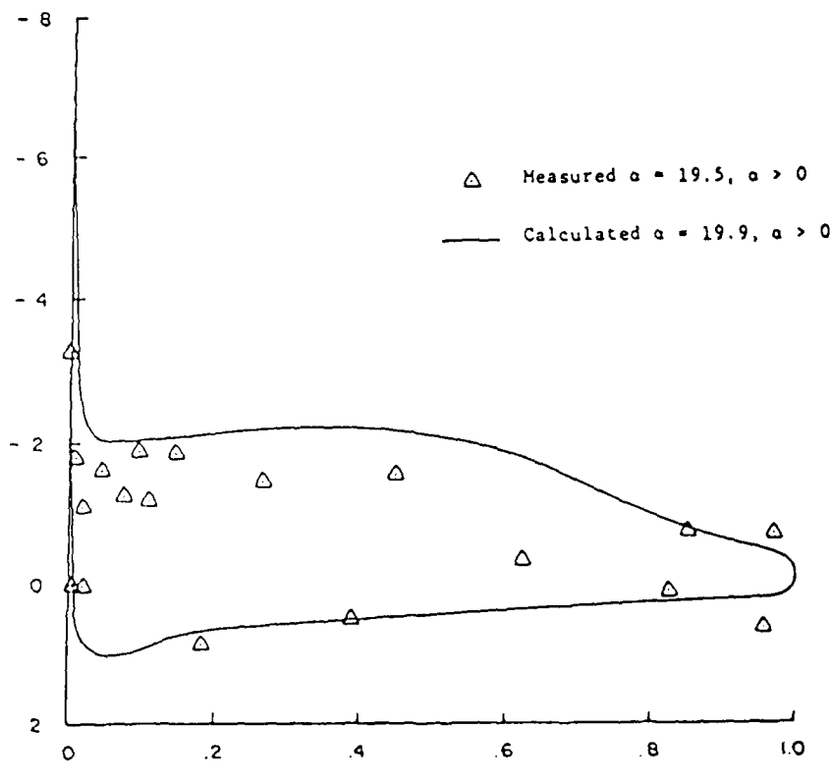

Figure 7.

Pressure coefficient comparison - NACA 0012 airfoil.

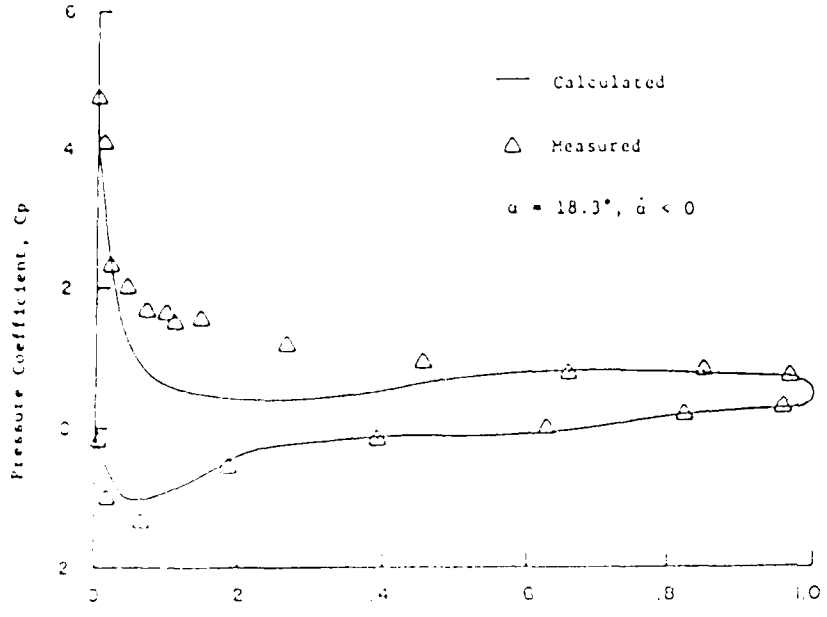

Figure 8.

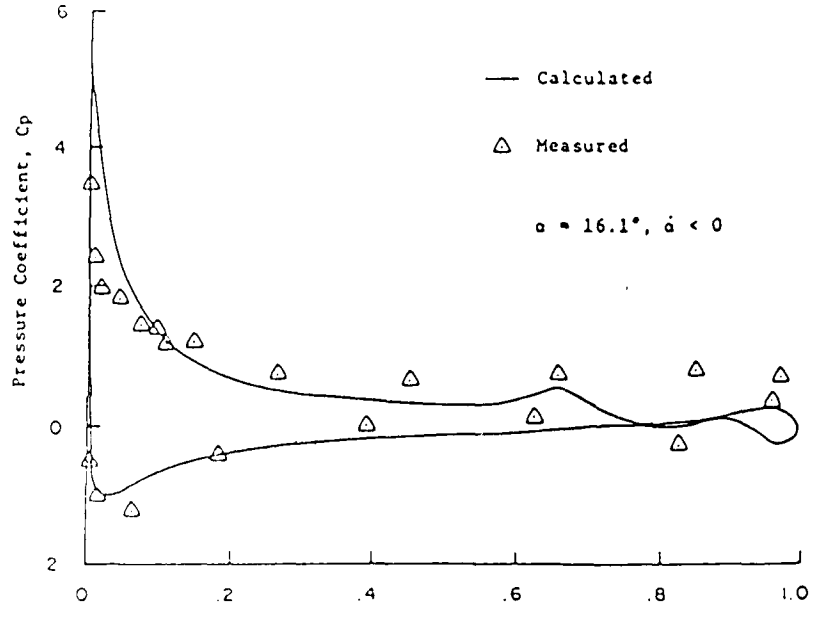

Figure 9.

Pressure coefficient comparison - NACA 0012 airfoil.

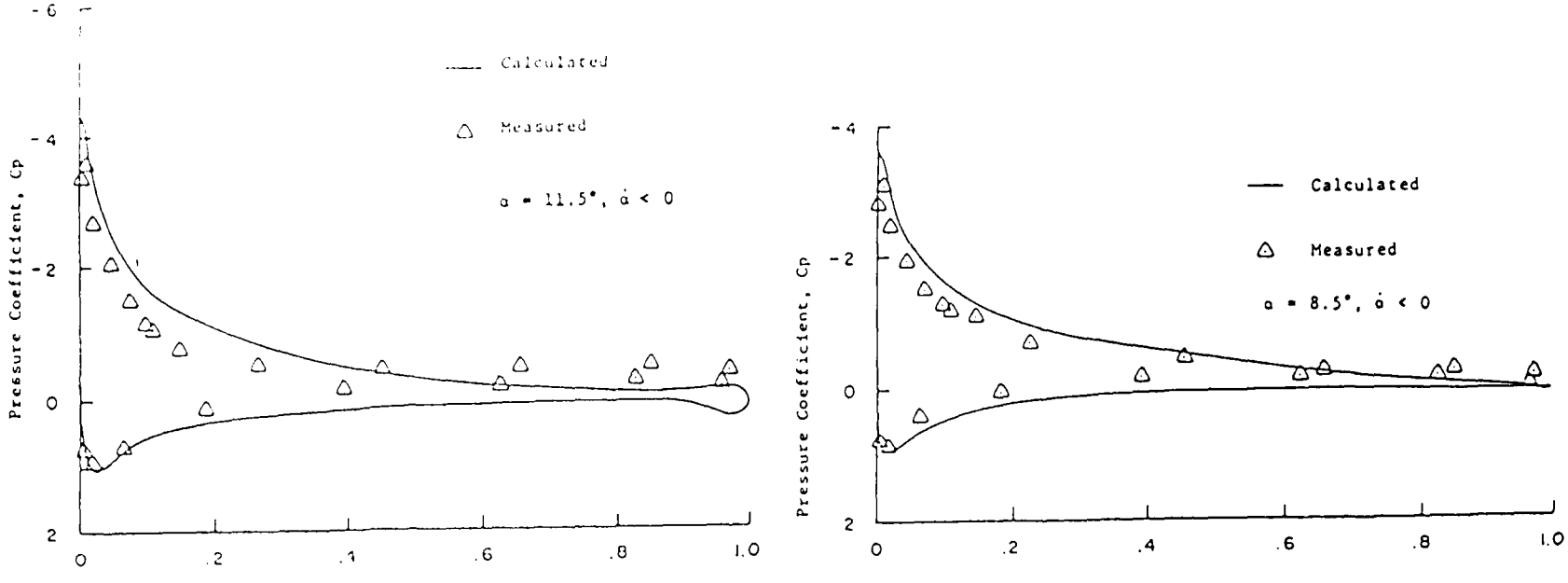

Figure 10. Pressure coefficient comparison - NACA 0012 airfoil.

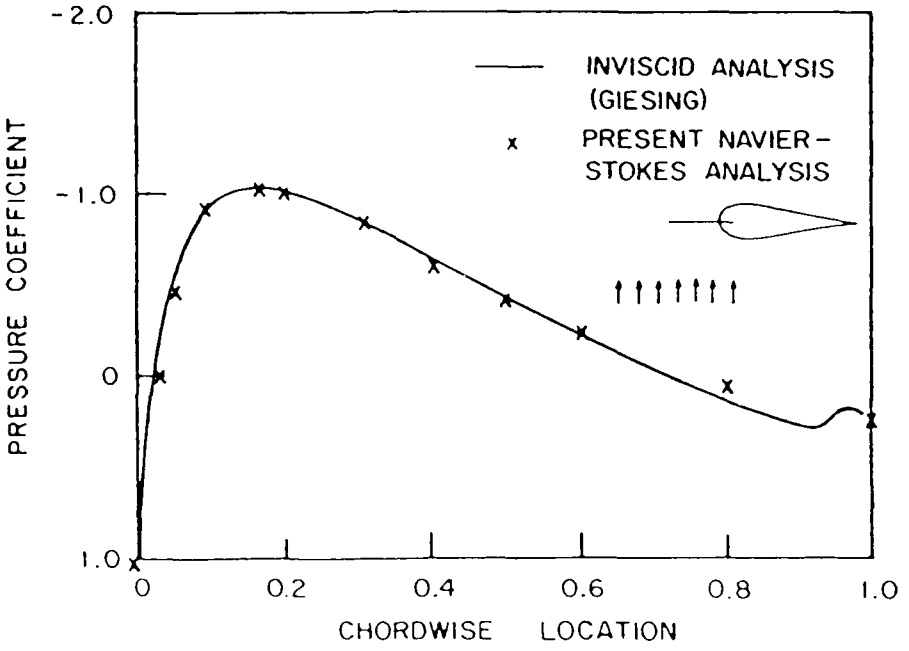

FIGURE 11. PRESSURE COEFFICIENT FOR 0.255 THICK JOUKOWSKI AIRFOIL ENTERING GUST, $T = -\infty$

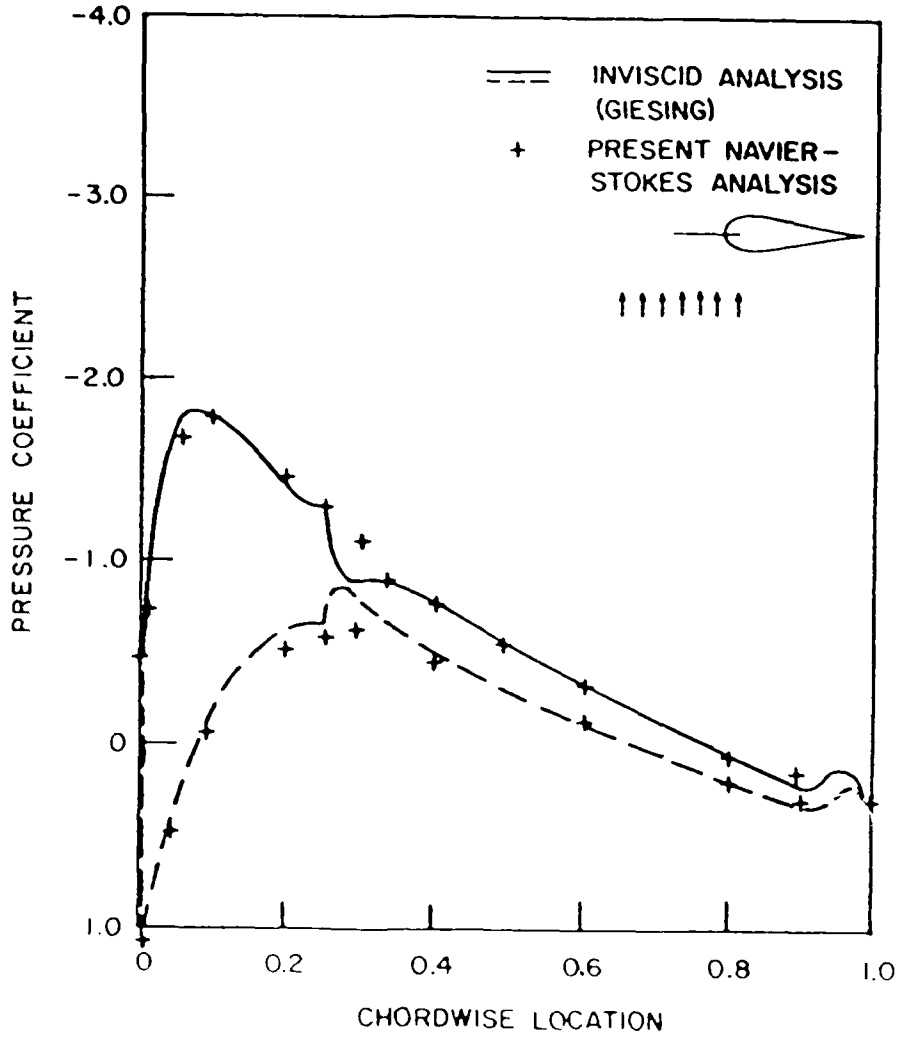

FIGURE 12. PRESSURE COEFFICIENT FOR 0.255 THICK JOUKOWSKI AIRFOIL ENTERING GUST, T = 0.25

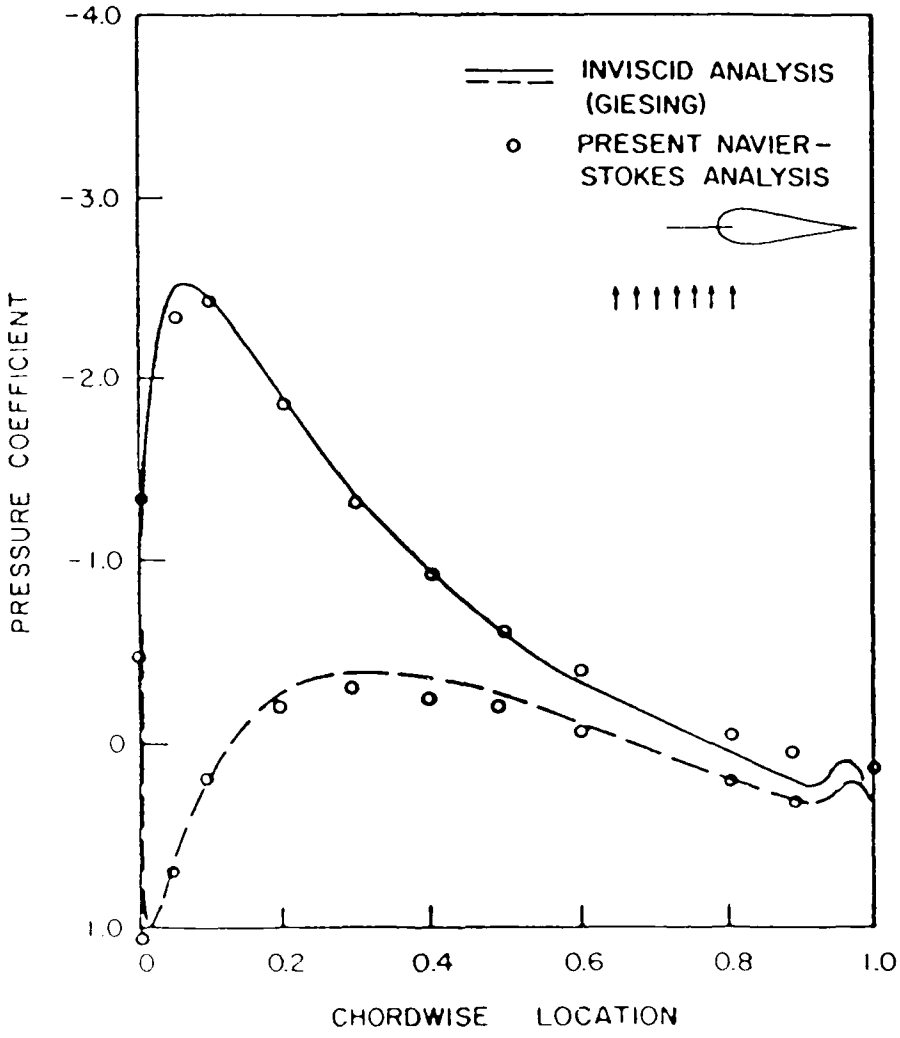

FIGURE 13. PRESSURE COEFFICIENT FOR 0.255 THICK JOUKOWSKI AIRFOIL ENTERING GUST, T = 1.00

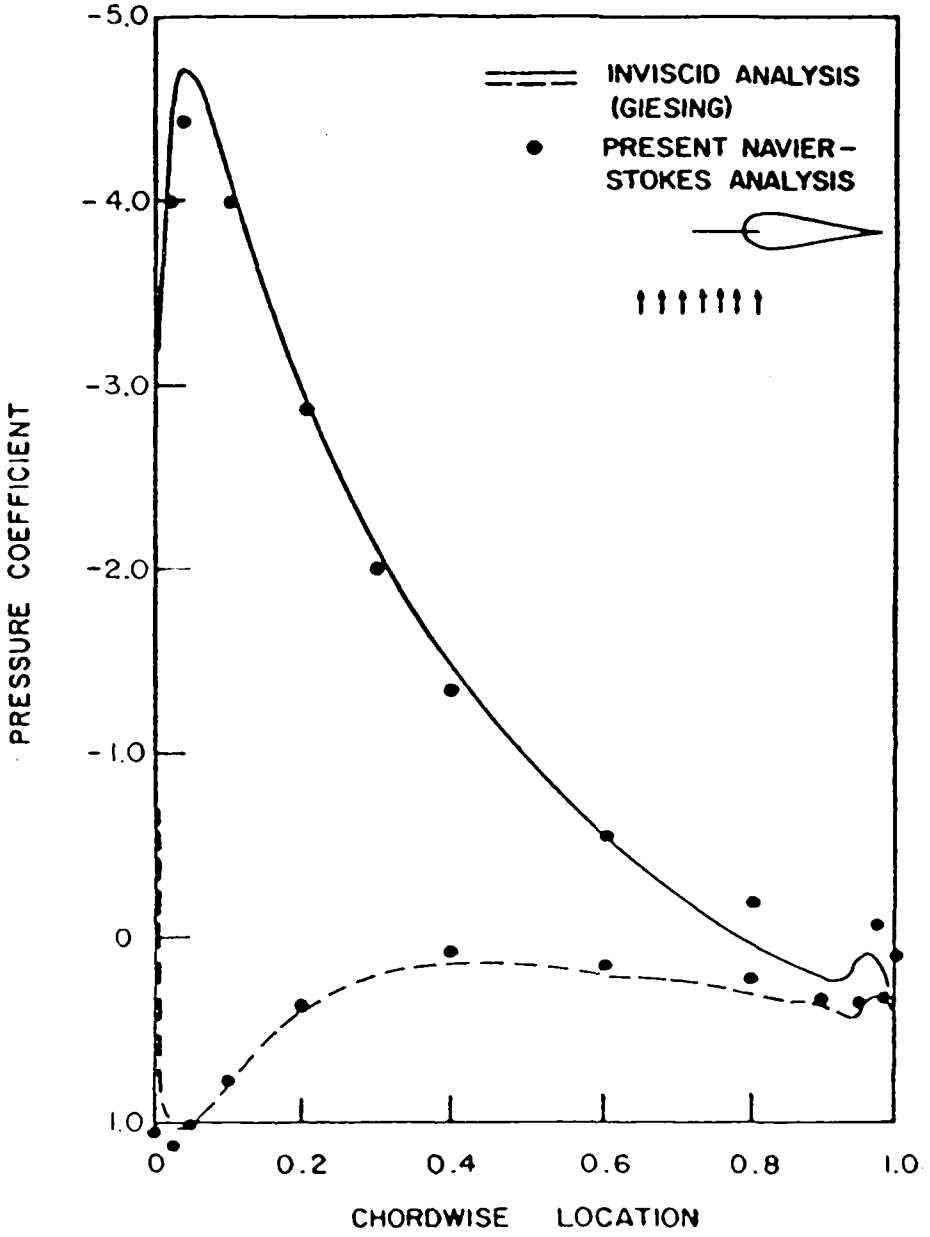

FIGURE 14. PRESSURE COEFFICIENT FOR 0.255 THICK JOUKOWSKI AIRFOIL ENTERING GUST, $T = \infty$

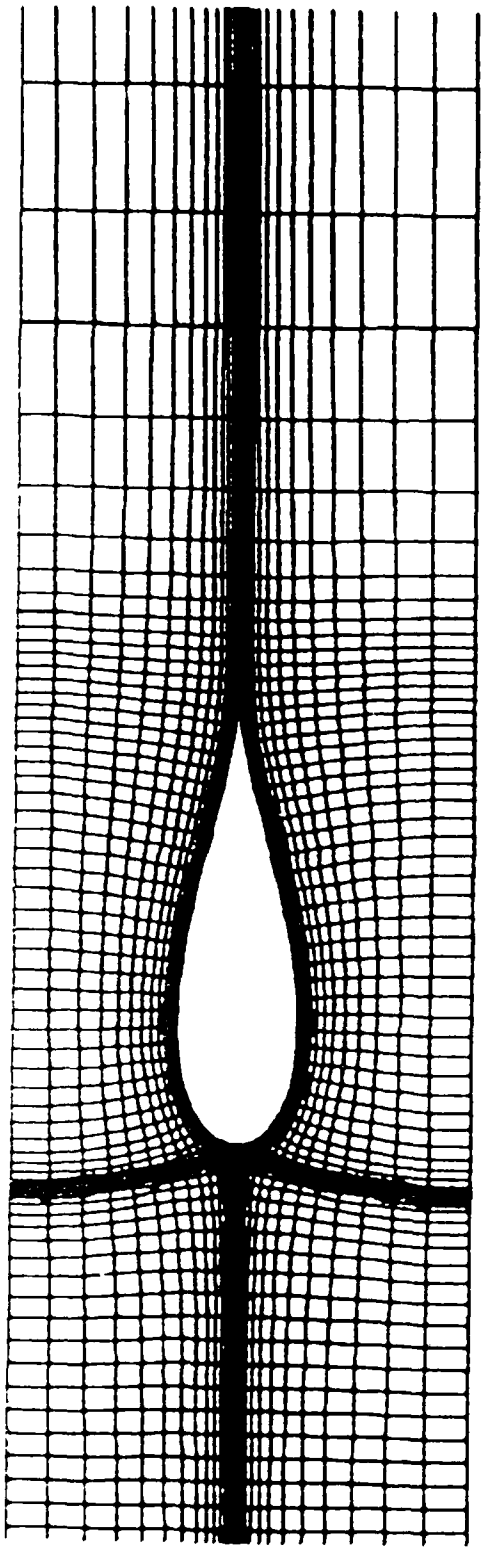

Figure 15. H-Grid Joukowski Cascade.

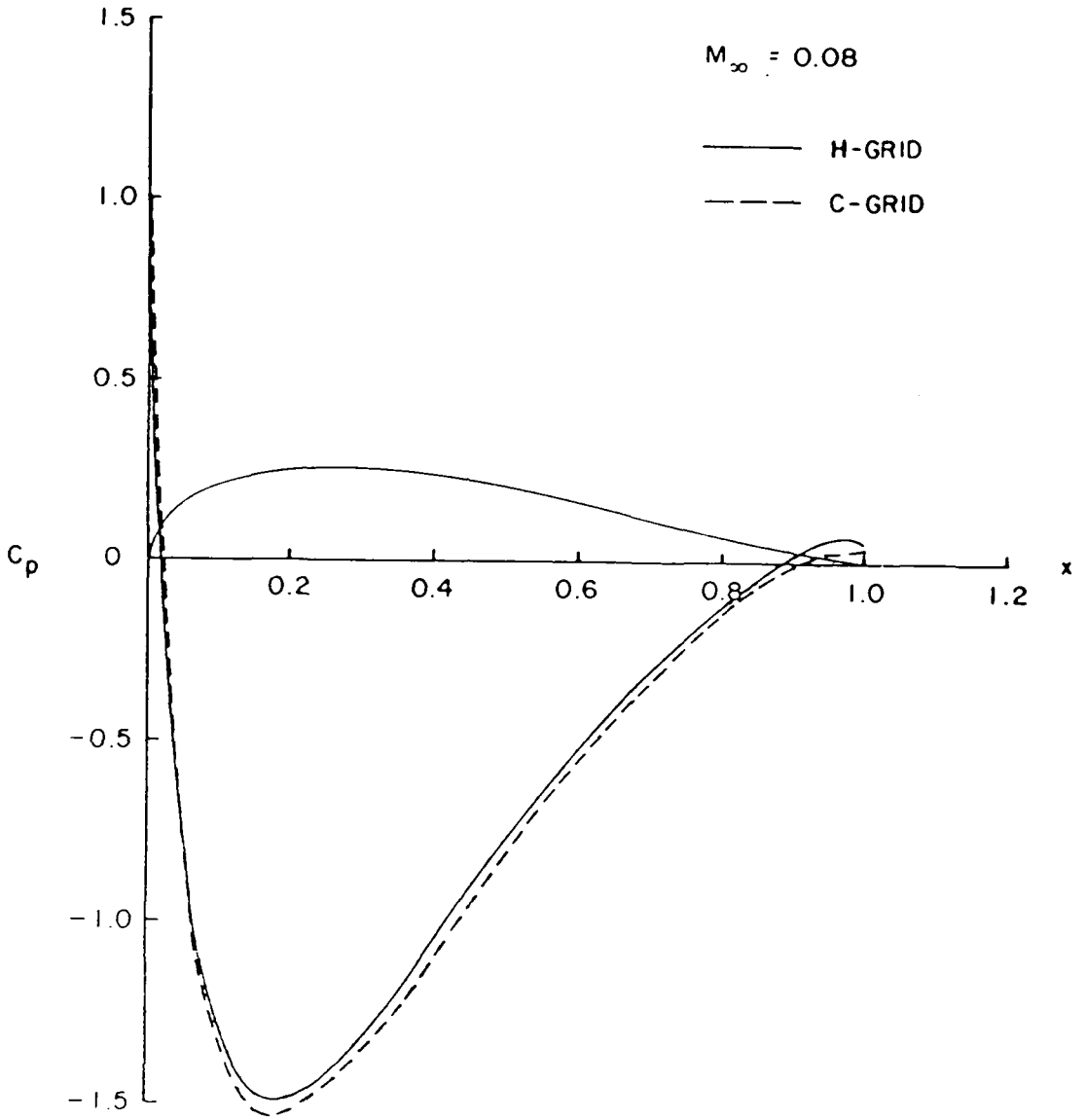

Figure 16. Comparison of pressure distributions, Joukowski Cascade.

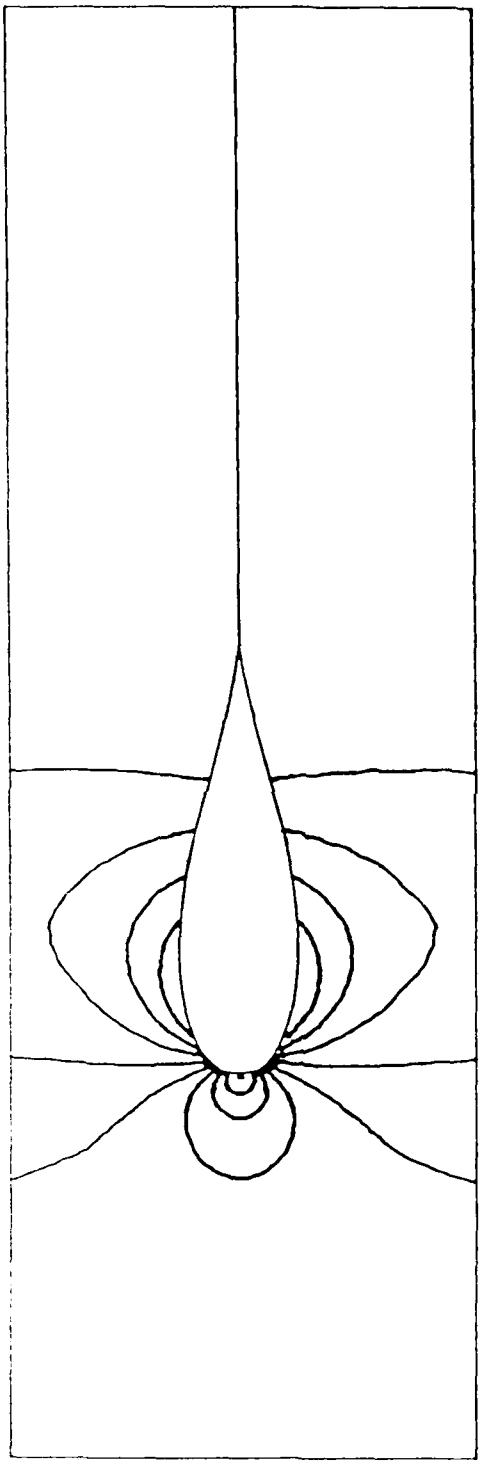

Figure 17. Pressure contours, H-Grid, Joukowski Cascade.

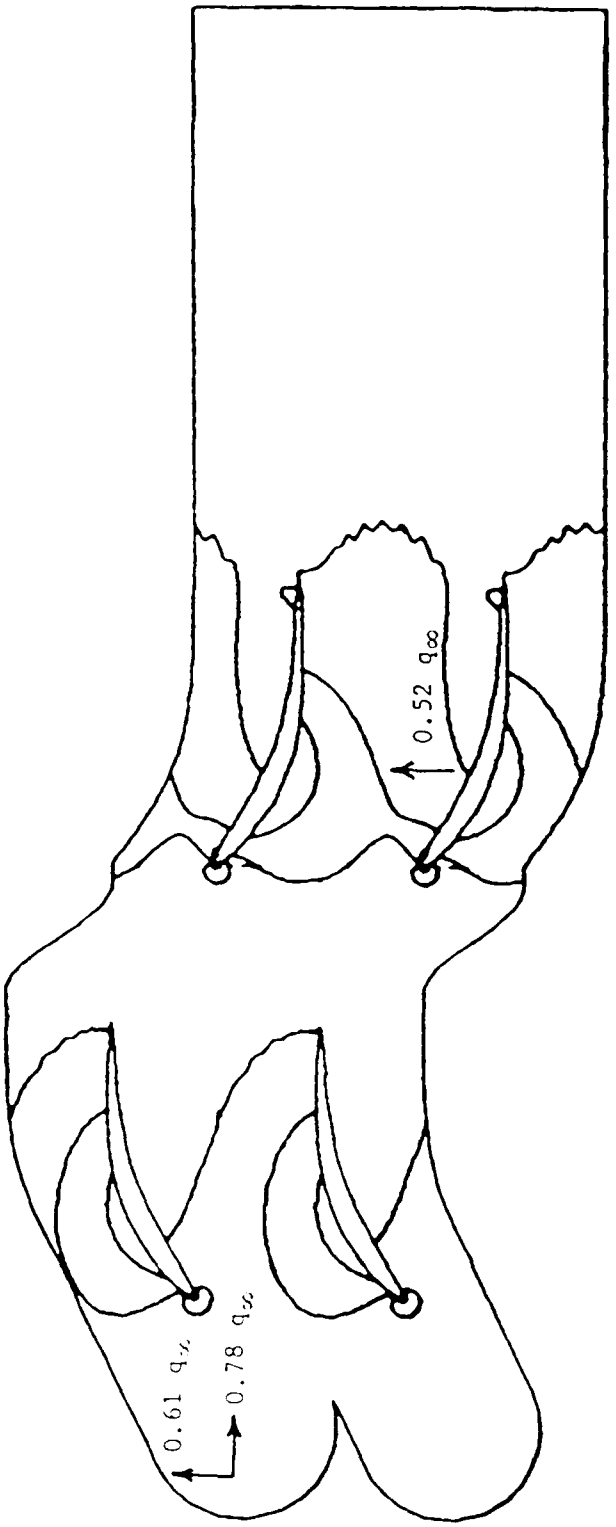

Figure 18. Inflow and blade velocity.

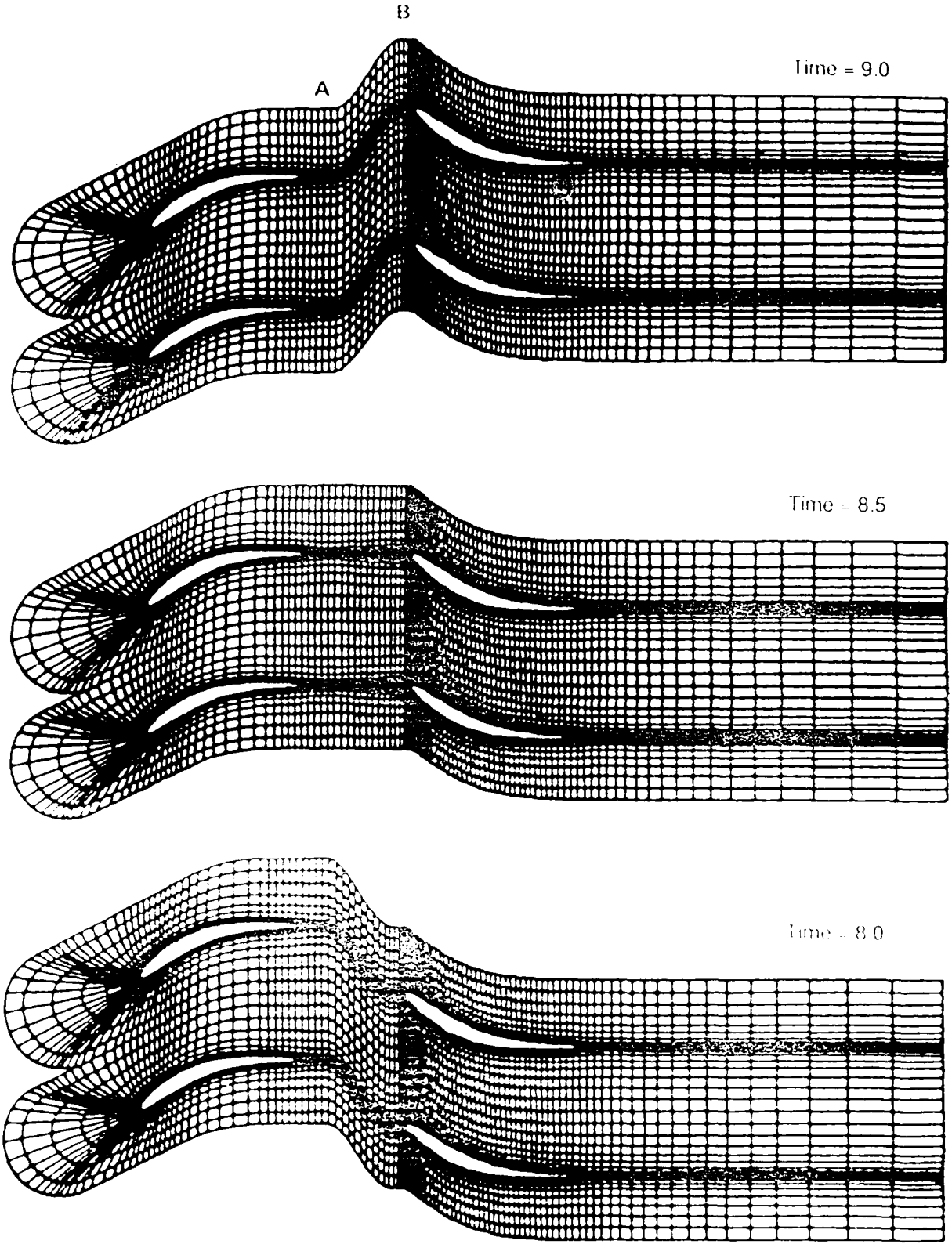

Figure 5-4. Boundary coordinate system for the Stephens - Hobby Cylinder

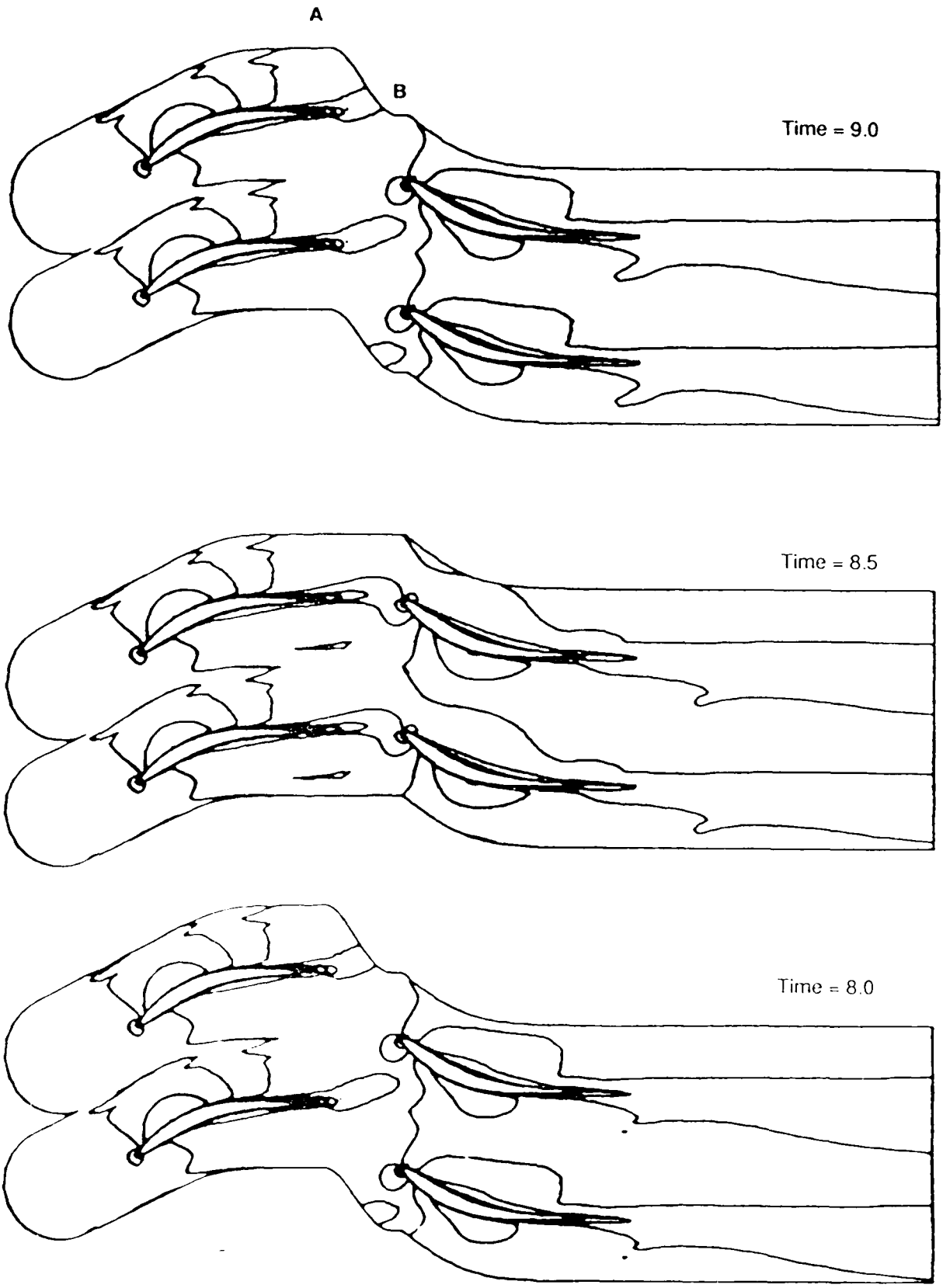

Figure 20. Mach number contours for the Stephens - Hobbs Cascade.

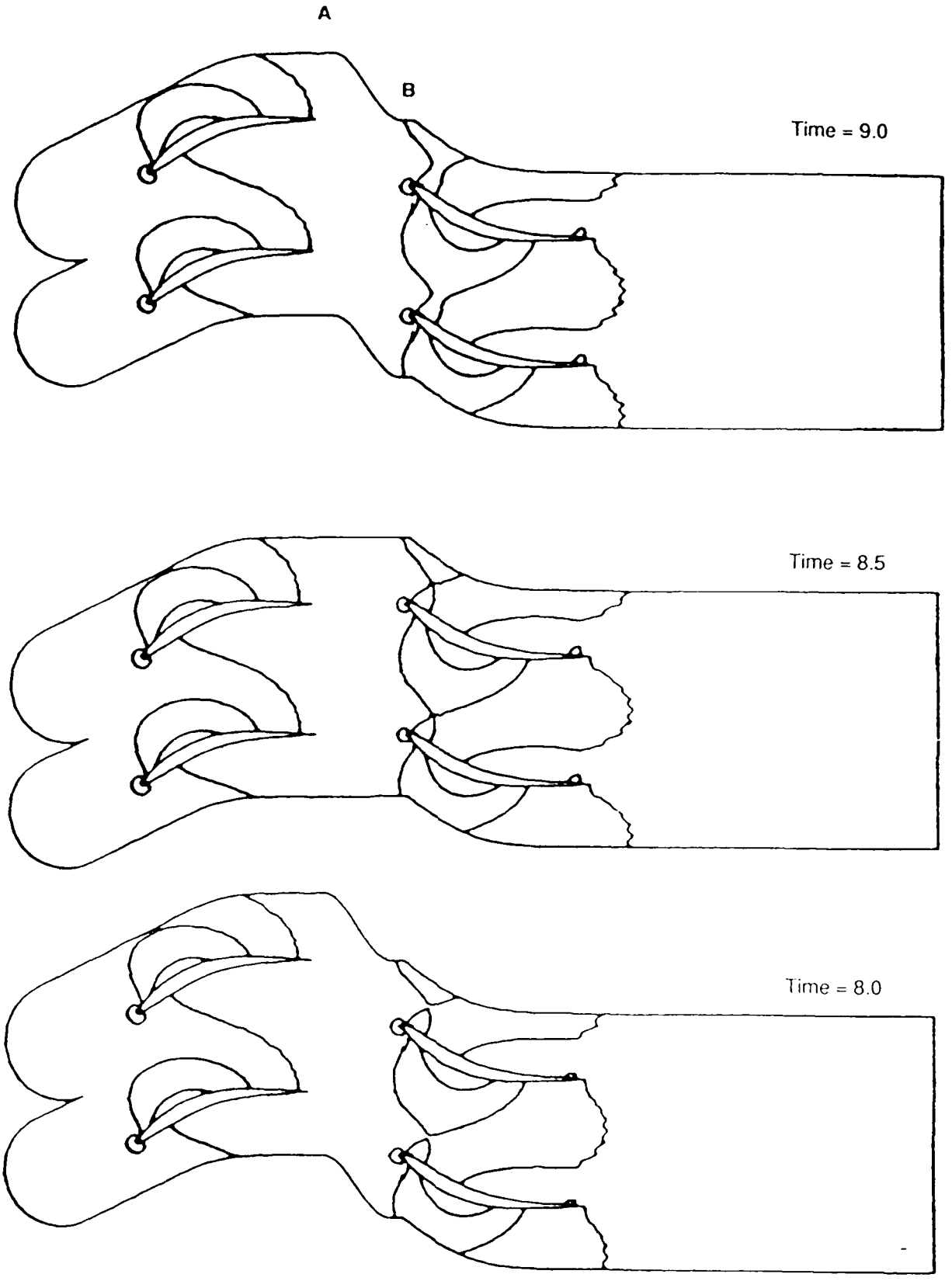

Figure 21. Static pressure contours for the Stephens - Hobbs Cascade.

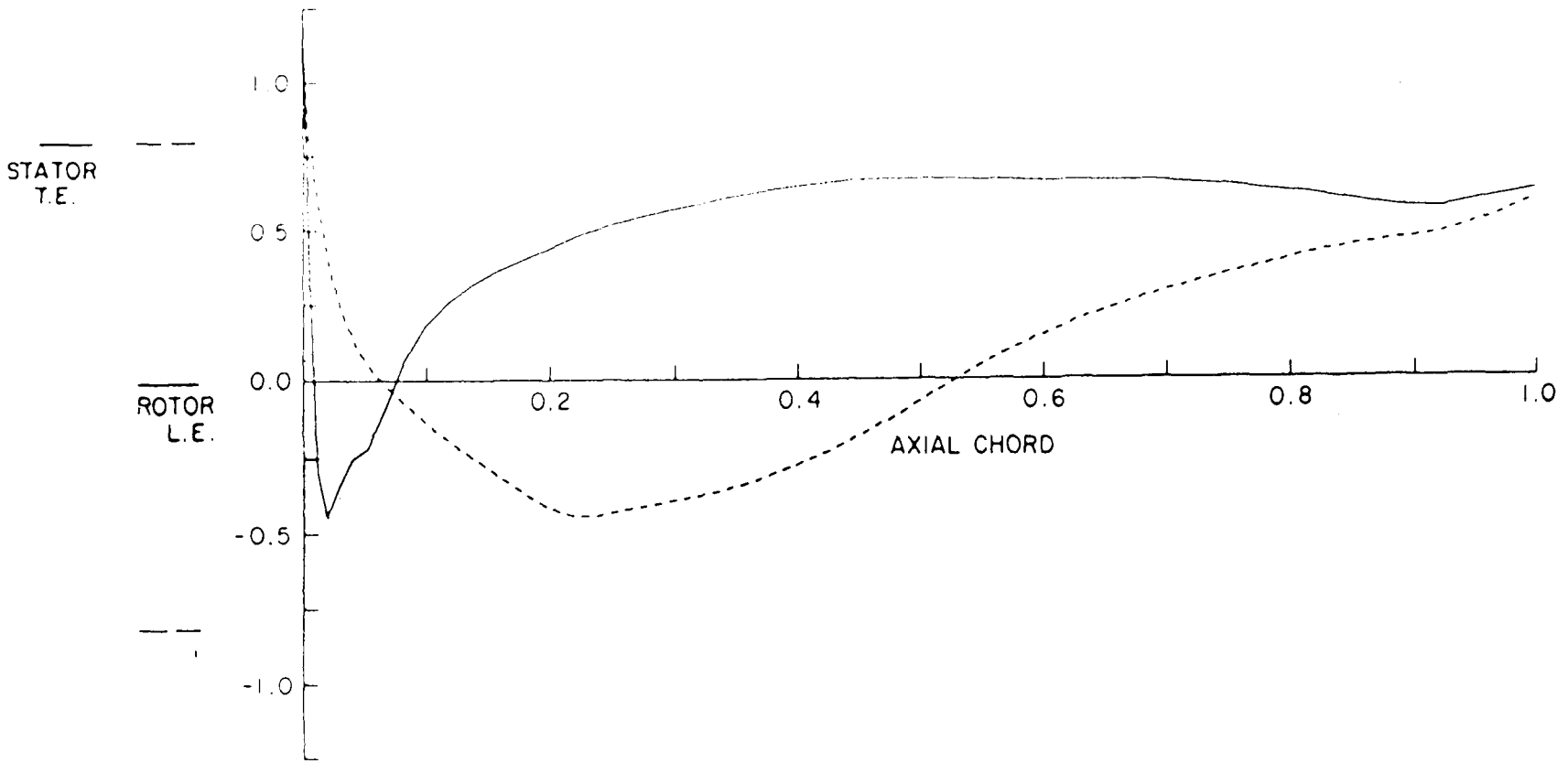

Figure 22. Rotor pressure coefficient perturbation, time = 8.00.

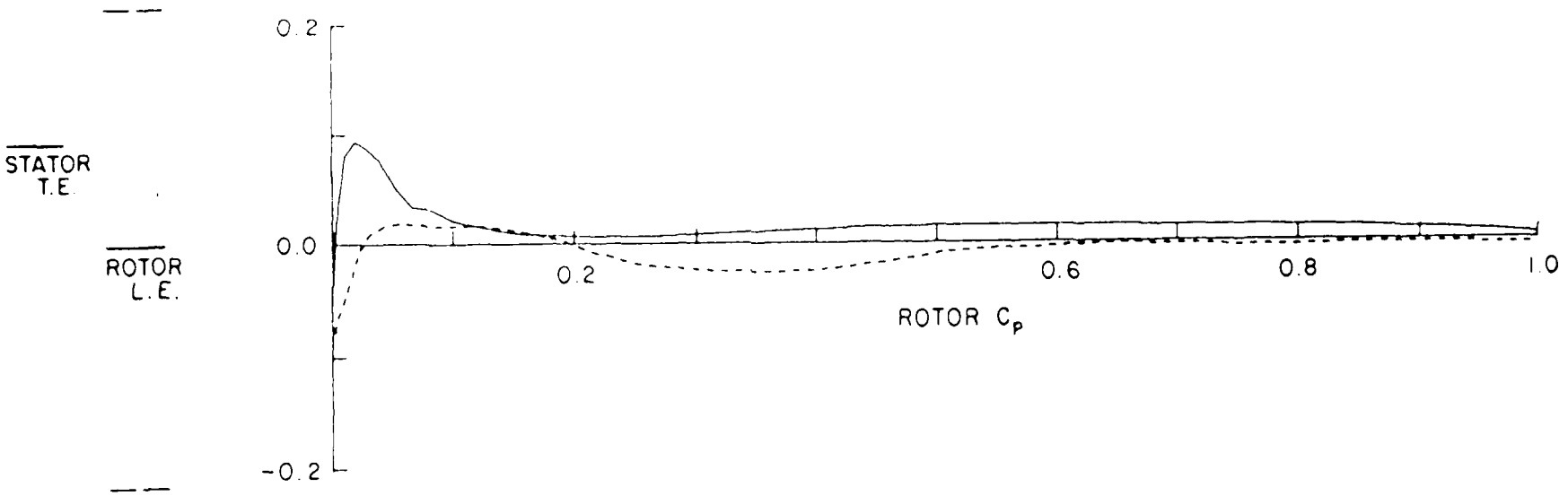

Figure 23. Rotor pressure coefficient perturbation, time = 8.29.

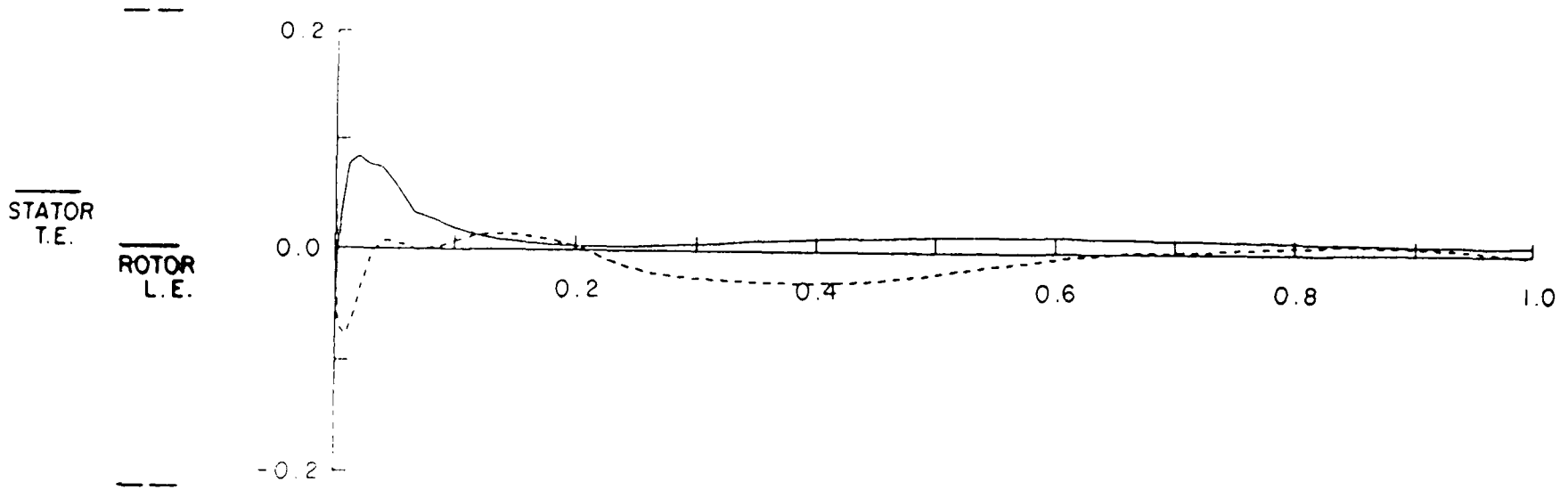

Figure 24. Rotor pressure coefficient perturbation, time = 8.39.

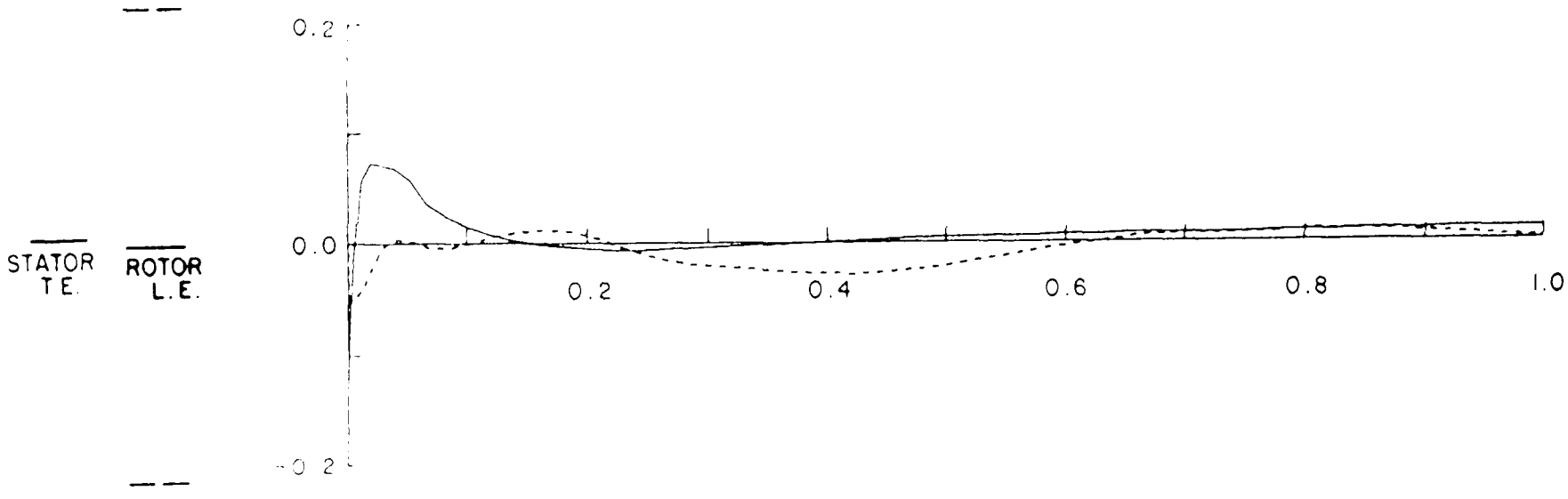

Figure 25. Rotor pressure coefficent perturbation, time = 8.49.

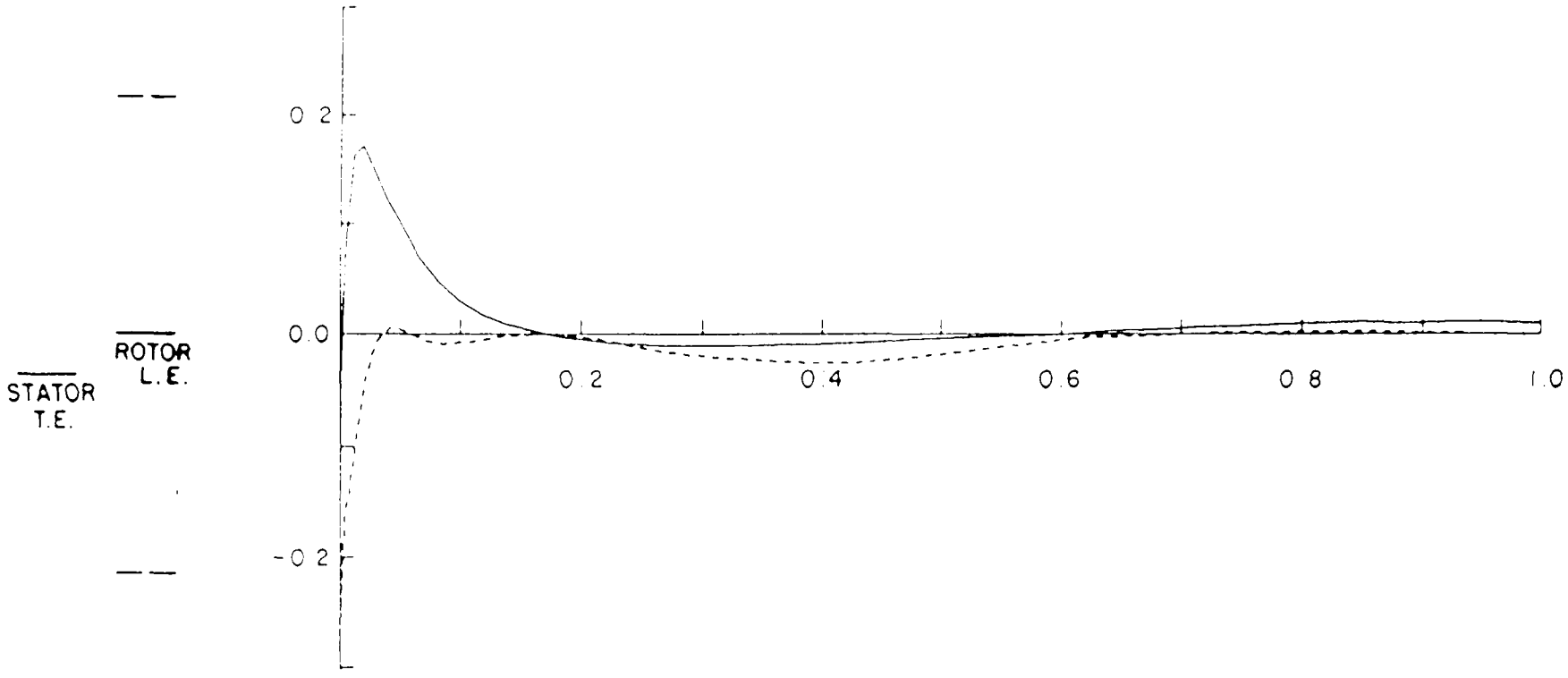

Figure 26. Rotor pressure coefficient perturbation, time = 8.59.

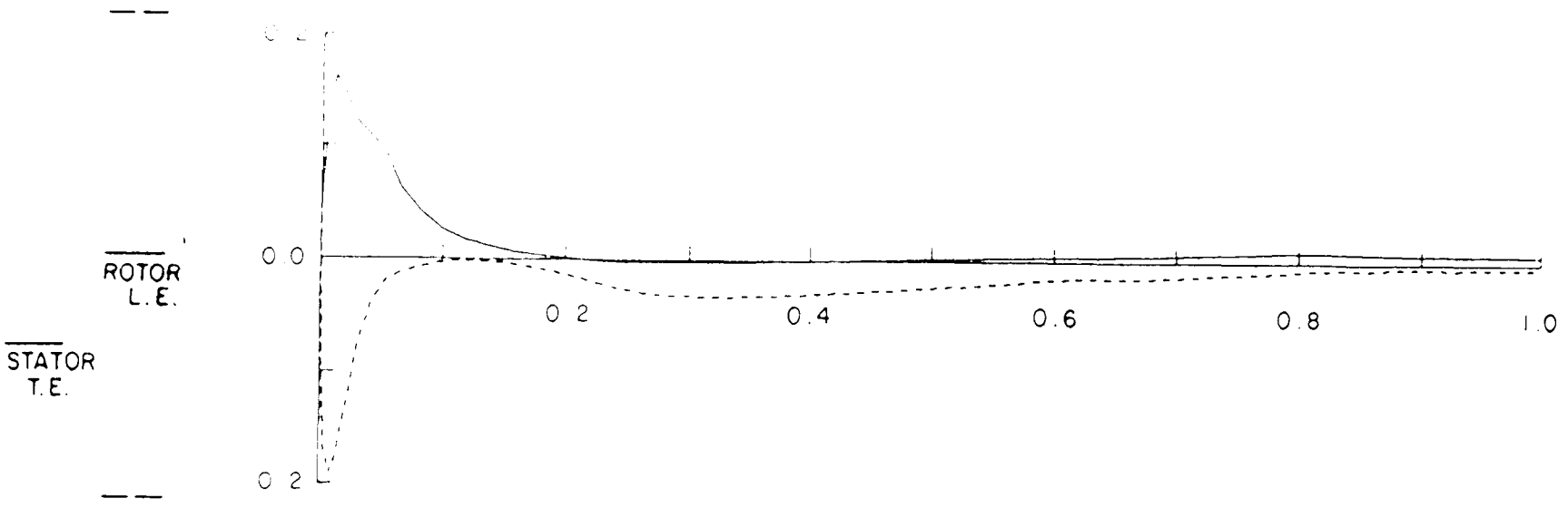

Figure 27. Rotor pressure coefficient perturbation, time = 8.69.

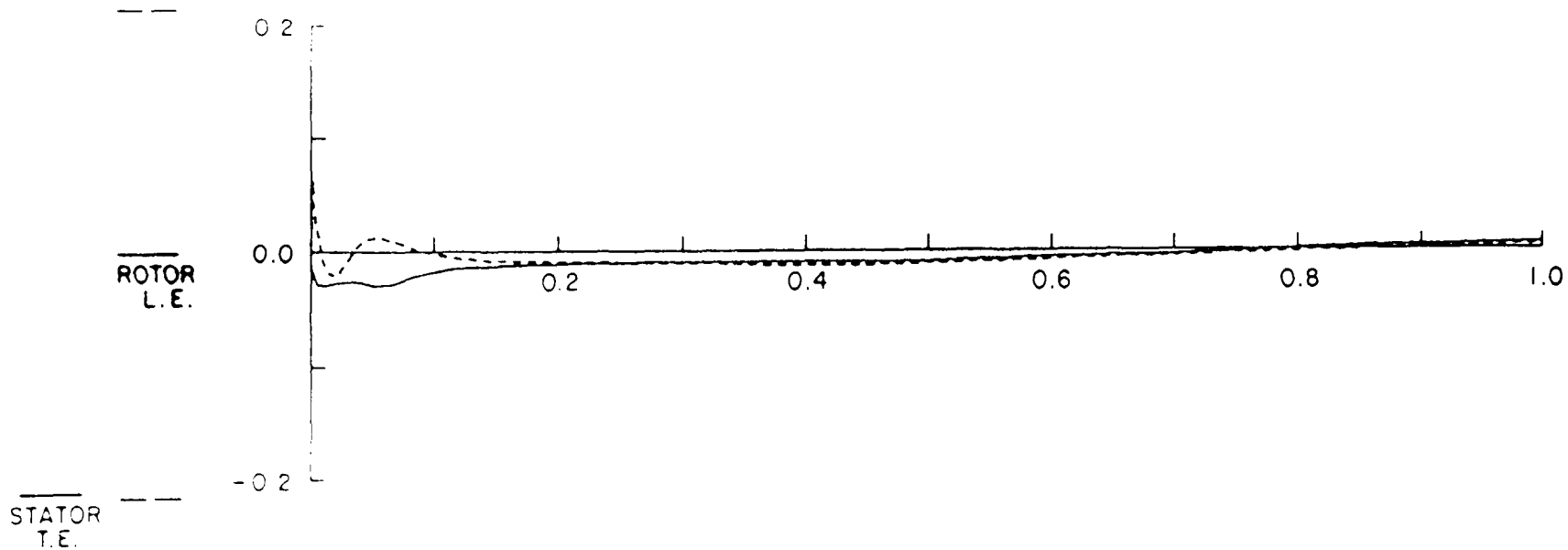

Figure 28. Rotor pressure coefficient perturbation, time = 8.99.

END

1-87

DTIC